Check for updates

Paraventricular nucleus CRH neurons encode stress controllability and regulate defensive behavior selection

Núria Daviu[1], Tamás Füzesi[1,2], David G. Rosenegger[1], Neilen P. Rasiah[1], Toni-Lee Sterley[1], Govind Peringod[1] and Jaideep S. Bains [1 ✉]

In humans and rodents, the perception of control during stressful events has lasting behavioral consequences. These consequences are apparent even in situations that are distinct from the stress context, but how the brain links prior stressful experience to subsequent behaviors remains poorly understood. By assessing innate defensive behavior in a looming-shadow task, we show that the initiation of an escape response is preceded by an increase in the activity of corticotropin-releasing hormone (CRH) neurons in the paraventricular nucleus (PVN) of the hypothalamus (CRH[PVN] neurons). This anticipatory increase is sensitive to stressful stimuli that have high or low levels of outcome control. Specifically, experimental stress with high outcome control increases CRH[PVN] neuron anticipatory activity, which increases escape behavior in an unrelated context. By contrast, stress with no outcome control prevents the emergence of this anticipatory activity and decreases subsequent escape behavior. These observations indicate that CRH[PVN] neurons encode stress controllability and contribute to shifts between active and passive innate defensive strategies.

The ability of any organism to respond to an immediate threat is critical for survival. Although specific defensive actions are genetically encoded and 'hardwired', each threat forces the individual to prioritize one behavior over others, or sequence multiple behaviors, which effectively creates a strategy for future challenges. Successful outcomes during repeated exposure to the same challenge reinforce successful strategies. This can be extremely advantageous and may contribute to long-term adaptive changes and encoding of traits that are inherited. Some experiences, however, can lead to maladaptive shifts in behavior. There are multiple features of the experience that lead to adaptive versus maladaptive behavioral changes. In humans, the severity of a trauma, its predictability and the perception of control over the outcome are all linked to enduring shifts in behavior and physiology[1,2]. Stress controllability is also a strong predictor of behavioral consequences in rodents; specifically, the level of outcome control during stress exposure is inversely related to the development of negative behavioral consequences[3]. The absence of control during stress contributes to the emergence of 'learned helplessness'[4], while control is linked to more active coping strategies associated with resilience[3]. Importantly, although there is a generalization to situations that are unrelated to the original experience, all of the work to date has focused on shifts in conditioned or learned behavioral strategies[5]. The neural substrates linking controllability to innate behaviors remain poorly understood.

The CRH[PVN] neurons are the canonical controllers of the endocrine response to stress. Recent work has revealed a number of previously unknown roles for these cells in stress-related behaviors that are independent of hormonal actions. In mice, this includes stress-induced grooming[6] and anxiety-like behaviors[6–9], which are consistent with a role for this system in facilitating stress coping following the initial challenge. Other studies highlight the importance of CRH[PVN] cells in initiating more active responses to the

stress. In mice, they are required for the release of alarm chemosignals to alert others to threat[9], whereas in larval zebrafish, activation of a homologous corticotropin system results in rapid locomotive behavior and avoidance to a variety of stressors[10]. This latter finding indicates that these cells may be an important component of the evolutionarily conserved 'flight' or escape response to a perceived threat. Recent work has speculated that activation of these neurons in rodents may also trigger rapid defensive behavior[11]. Collectively, these observations demonstrate that CRH[PVN] neurons are central for both responding to and coping with stress. Although the endocrine response to stress is insensitive to relative behavioral control during prior stressful events[12], PVN neurons show differential *c-fos* responses to controllable and uncontrollable stress[13], which suggests that they may be important in encoding information related to stress controllability.

Here, we hypothesized that CRH[PVN] neurons link stress controllability and escape behavior. We combined in vivo fiber photometry with different threat paradigms that trigger innate (unlearned) escape behaviors and then used modified instrumental training in which the subject either has control over the outcome or has no control over the outcome to assess the activity of CRH[PVN] neurons. We took advantage of recent developments in the looming and advancing predator model[14] to test the consequences of controllability training on escape behavior. Our data reveal that an increase in the activity of CRH[PVN] neurons precedes escape behavior and that the ability of these cells to encode controllable and uncontrollable stress differentially modifies innate defensive strategies, even in unrelated contexts in the future.

Results

CRH[PVN] neurons modulate defensive behaviors to a looming shadow. We investigated innate defensive and survival behaviors in

[1]Hotchkiss Brain Institute and Department of Physiology and Pharmacology, University of Calgary, Calgary, Alberta, Canada. [2]CSM Optogenetics Core Facility, Cumming School of Medicine, University of Calgary, Calgary, Alberta, Canada. ✉e-mail: jsbains@ucalgary.ca

mice using an experimental paradigm that mimics a looming threat that descends from the sky. The expansion of a virtual shadow above the arena mimics the approach of a predator from the sky. This increase in threat imminence initiates defensive behavior: either a targeted escape to a shelter or freezing. Laboratory mice do not have prior experience with this particular task (task-naive), so their behavioral response reflects a choice from a repertoire of unlearned or innate defensive behaviors. In this study, mice were allowed to habituate to the test arena, which was equipped with a rudimentary shelter, for three successive days (Fig. 1a,b). The virtual shadow was a black disk that appears in the 'sky' above the arena, hovers and then increases in size to mimic the looming and advancing of a descending predator. There were three phases to the 8-s stimulus presentation: (1) a 2-cm black disk appears static against a light gray background for 3 s; (2) the disk increases in size for 2 s; (3) it remains at maximum size (20 cm) for 3 s (Fig. 1c). On the test day, after 3 min of habituation in the arena, mice were subjected to five looming-shadow trials with an inter-trial interval of at least 1 min (Fig. 1d). The behavioral responses during each trial were classified into one of the three following categories (Fig. 1e): escape, freeze or no response. An escape was denoted when a flight behavior was initiated and the subject reached the shelter during the 8-s trial. A freeze response consisted of either the absence of movement during the full stimulus presentation or repeated, discontinuous bouts of freezing during the trial. Finally, non-responders showed no distinguishable response to the visual stimulus. The behavioral analysis of this task revealed that task-naive mice favored escape behavior targeted to the shelter (escape probability (P_{escape}) = 0.78) over freezing or no-response (no escape probability ($P_{no\ escape}$) = 0.22); Fig. 1f–h), which suggests that there is a bias toward an active defensive strategy in response to a possible advancing threat from above.

To determine whether these strategies are flexibly modified by prior experience, we repeated the experiment in the same mice 22 days after the original exposure (Extended Data Fig. 1a). We

hypothesized that since the paradigm did not deliver an actual threat, mice should modify their behaviors to more passive behaviors during a subsequent challenge. Consistent with our hypothesis, the second set of trials resulted in less frequent escape behaviors (P_{escape}: 0.55 versus 0.78 for task-naive mice (Fisher's exact test, two-tailed, $P = 0.0149$) and an increase in the non-responders (Extended Data Fig. 1b–e). This suggests that these mice learn from the original experience and that the absence of an actual threat results in behavioral modification. To determine whether CRH[PVN] neurons

Fig. 1 | CRH[PVN] neurons modulate defensive behaviors to a looming shadow. **a**, Protocol for the looming-shadow experiment. **b**, Cartoon of the looming-shadow test apparatus with a mouse and shelter. **c**, Schematic representation of the visual stimulus. **d**, Repeated looming-shadow test protocol: five trials, each consisting of a single looming stimulus, were delivered with an inter-trial interval of >1 min. **e**, Pictorial representation of behavioral outputs analyzed. Escape (blue) was defined as a flight response targeting the shelter during stimulus presentation; freezing (green) was defined as the absence of movement during the stimulus presentation, including discontinuous freezing episodes; no response (gray) was defined as no distinguishable response to the visual stimulus. **f**, Individual trials ($n = 55$ trials, $N = 11$ mice). **g**, Behavioral summary of trials. **h**, Representation of the starting location in the chamber for each individual trial. **i**, Top: schematic of the injected viral construct. Bottom: viral injection and ferrule implantation strategy for photoinhibition experiments. **j**, Example of confocal image showing expression of Cre-dependent AAV-DIO-Arch3.0-eYFP virus in tdTomato-positive CRH[PVN] neurons. **k**, Representative whole-cell recording from a CRH[PVN] neuron in a brain slice, demonstrating spike suppression in response to 532-nm light. **l**, Looming-shadow experimental protocol for the CRH[Arch3.0] experiment. Photoinhibition of CRH[PVN] cells occurred during 3 min of habituation and five trials of the looming shadow. **m**, Individual trials ($n = 40$ trials, $N = 8$ mice for each group) of the behavior in mice expressing either eYFP or Arch3.0 in CRH[PVN] neurons. **n**, Behavioral summary of trials. **o**, Data compiled and presented as the fraction of trials in each mouse showing a decrease in escape ($n = 40$ trials, $N = 8$ mice for each group) (two-tailed unpaired Mann–Whitney test, $U = 12.5$, $P = 0.0413$), an increase in freezing (two-tailed unpaired Mann–Whitney test, $U = 6$, $P = 0.0044$) and no difference in the non-responders (two-tailed unpaired Mann–Whitney test, $U = 19$, $P = 0.1795$). Data shown represent the mean ± s.e.m.
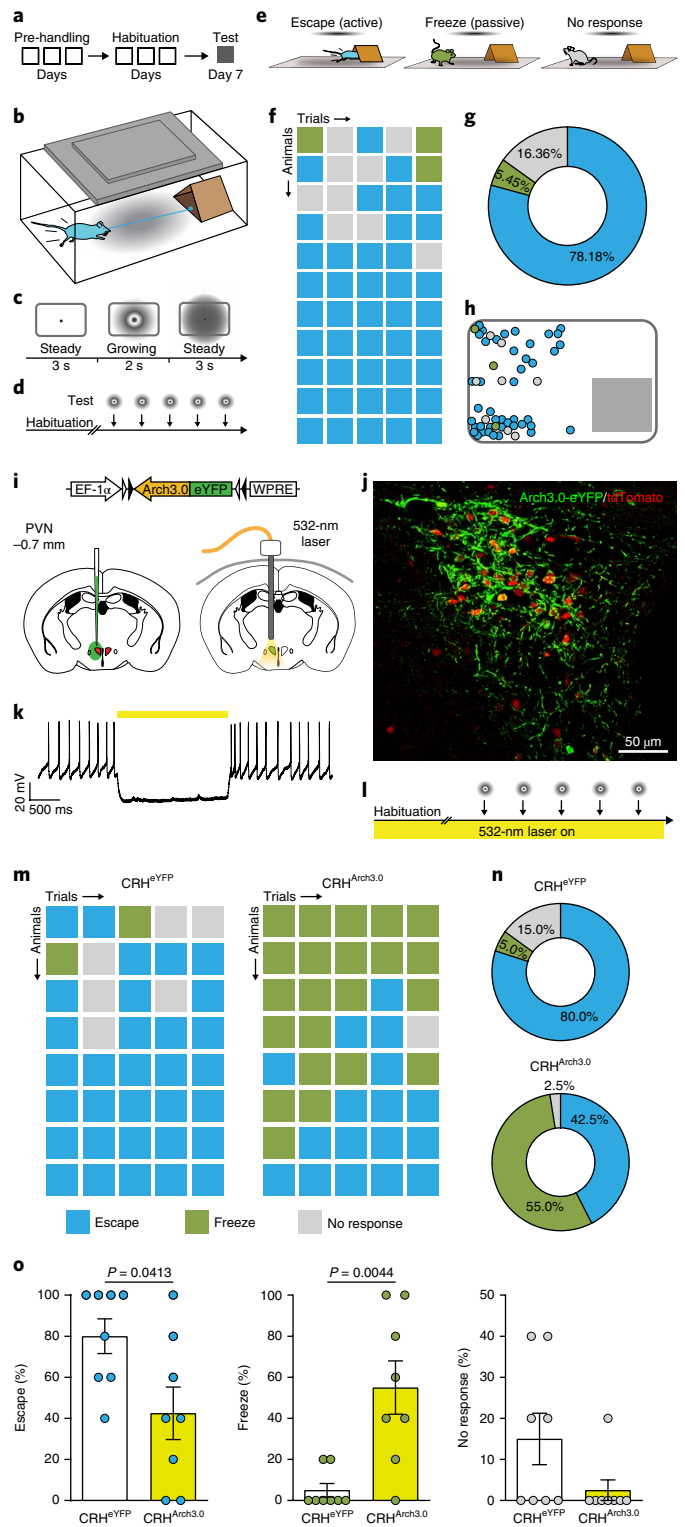
are involved in the execution of the behavioral strategy in response to a looming shadow, we performed a targeted activity silencing experiment (Fig. 1i,j). We transfected CRH[PVN] neurons in one group of mice with the light-sensitive proton pump archaerhodopsin 3.0 (CRH[Arch3.0])[15], and a control group with enhanced yellow fluorescent protein (CRH[eYFP]). We performed whole-cell recordings in CRH neurons in hypothalamic brain slices to test the effects of CRH[Arch3.0] neuron inhibition. Consistent with our previous findings[6,9], delivery of light (532 nm) hyperpolarized the neurons, resulting in a decrease in spike activity (Fig. 1k and Supplementary Fig. 1). CRH[Arch3.0] or CRH[eYFP] mice were placed in the shadow test arena and yellow light was delivered continuously during the looming-shadow test (Fig. 1l). As with the naive mice, CRH[eYFP] mice showed a bias toward active defensive behavior, exhibiting an escape response in 80% of the trials. By contrast, there was a decrease in escape behavior in CRH[Arch3.0] mice (42.5% of trials) and an increase in freezing behavior (55% of trials; Fig. 1m–o and Extended Data Fig. 1f). These experiments demonstrate that behavioral strategies can be modified either by prior experience or by photoinhibition of CRH[PVN] neurons. Previous experience with the looming shadow caused a shift from escape behavior toward indifference (no response), which suggests that these mice exhibit experiential learning. Meanwhile, silencing CRH[PVN] neuron activity also decreased escape, but shifted the behavioral choice toward freezing. These findings indicate that the activity of CRH[PVN] neurons controls the balance between passive and active strategies in response to an increase in threat imminence.

Increase in CRH[PVN] neuron activity during looming or advancing threat. In most animals, increases in the output of the hypothalamic–pituitary–adrenal axis are an essential component of the response to both acute and persistent stress. In rodents, numerous studies have established clear links between acute stress and an increase in circulating stress hormones, but there is limited information on the activity of CRH[PVN] neurons in freely behaving animals. Here, we used fiber photometry to assess changes in Ca^{2+} levels in CRH[PVN] neurons. Using a viral strategy, we specifically expressed the genetically

encoded Ca^{2+} reporter GCaMP6s in CRH[PVN] neurons (CRH[GCaMP]; Fig. 2a,b). We implanted an optical fiber and used photometry[16,17] to record Ca^{2+} changes in CRH[PVN] neurons as a proxy of population activity (Fig. 2c and Supplementary Fig. 2). To test the reliability of this approach, we obtained signals from the fiber in response to footshock (FS). This stimulus increases CRH[PVN] neuron activity[11] and drives corticosterone release[9]. We observed a consistent
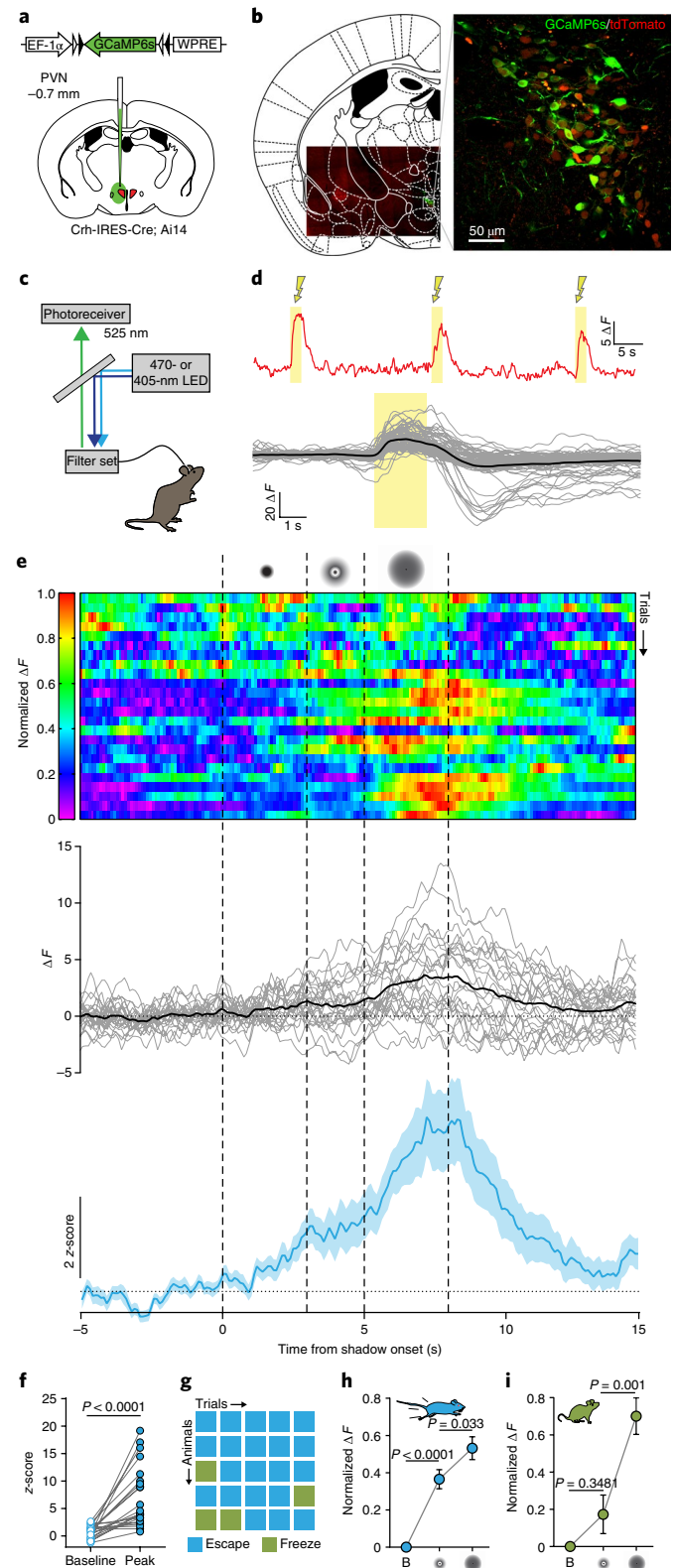

Fig. 2 | Increase in CRH[PVN] neuron activity during a looming or advancing threat. a, Top: schematic of the injected viral construct. Bottom: viral injection and ferrule implantation strategy for GCaMP6s in CRH[PVN] neurons. **b**, Coronal hemi-section map with an overlaid confocal image (expanded on the right) depicting GCaMP6s expression in CRH[PVN] neurons. **c**, Representation of single-fiber photometry method. **d**, Top: example trace of CRH[PVN] neuron activity (ΔF) during three consecutive FS stimuli. Bottom: individual traces (gray) and mean (overlaid, black) of CRH[PVN] neuron activity (ΔF) in response to a FS ($n = 80$ trials, $N = 8$ mice). **e**, Heatmap (top) and calcium traces (middle, ΔF) representing individual trials (gray); mean (overlaid, black) of CRH[PVN] neuron activity ($n = 25$ trials, $N = 5$ mice). Mean z-score of CRH[PVN] calcium response during visual stimulus (bottom). **f**, Individual z-scores for baseline (–5 to 0 s) and peak calcium response during the stimulus presentation (0–8 s) (paired t-test, two-tailed, $t(24) = 5.786$, $P < 0.0001$, 95% confidence interval (CI): 4.103 to 8.668). **g**, Individual trials showing behavior ($n = 25$ trials, $N = 5$ mice). **h**, Normalized ΔF peak for escape trials ($n = 21$ trials, $N = 5$ mice) during baseline (B) (–5 to 0 s), visual stimulus growth phase (3 to 5 s) and during fully grown fixed stage (5–8 s) (repeated-measures ANOVA, $F(1.919, 38.38) = 44.87$, $P < 0.0001$; Bonferroni's multiple comparisons test, baseline versus 3–5 s, $P < 0.0001$, 95% CI: –0.4995 to –0.2314; 3–5 s versus 5–8 s, $P = 0.0330$, 95% CI: –0.0329 to –0.01128). **i**, Normalized ΔF peak and for freeze trials ($n = 4$ trials, $N = 3$ mice) (repeated-measures ANOVA, $F(1.144, 3.431) = 37.49$, $P = 0.0056$; Bonferroni's multiple comparisons test, baseline versus 3–5 s, $P = 0.3481$, 95% CI: –0.6064 to –0.2600; 3–5 s versus 5–8 s, $P = 0.0010$, 95% CI: –0.6591 to –0.3956). Solid lines represent the average, and shaded areas indicate the s.e.m. Data shown represent the mean ± s.e.m.

increase in CRH[PVN] neuron activity in response to FS (Fig. 2d and Supplementary Fig. 3), which we in turn examined during the looming-shadow test. In task-naive mice, this increase in activity was evident during the appearance and subsequent expansion of the shadow (Fig. 2e,f). CRH[PVN] neuron activity was unaffected by either of the non-advancing visual stimulus, in which the disk moved laterally across the sky or was a static black disk (Extended Data Fig. 2a). The behavior analysis revealed a bias toward escape behavior (84% of the trials; Fig. 2g) that was not significantly different from naive non-instrumented mice (P_{escape}: 0.84 versus 0.78 for naive; Fisher's exact test, two-tailed, $P = 0.2795$). In the escape trials, the average speed was $17.4 \pm 2.3\,\mathrm{cm\,s^{-1}}$, which is in line with previous reports of velocities described for conditioned escape behavior in mice[18]. To investigate the link between behavioral output and CRH[PVN] neuron activity, we analyzed the calcium trace and behavior for each trial (Fig. 2h,i). Trials that resulted in an escape response showed an increase in the CRH[GCaMP] signal during the expansion phase of the stimulus[14]. By contrast, in the mice that exhibited freezing behavior, we did not observe an increase in the CRH[GCaMP] signal during the shadow-expansion phase, but did observe an increase in signal once the shadow had reached a stable full-expansion state (Extended Data Fig. 2d). These data, together with the observation that inhibition of CRH[PVN] neurons decreases escape behavior, suggest that CRH[PVN] activity is involved in the escape behavior observed in the looming-shadow test.

CRH[PVN] neurons anticipate the escape response to an imminent threat. The above data suggest a tantalizing link between CRH[PVN] neuron activity and the escape response to a looming shadow, but do not provide temporal information about the relationship. To extract this information, we used two different approaches to quantify the onset of flight behavior. In one, an independent observer scored videos of trials and determined the escape response time (ERT) as the moment at which the mouse made a movement toward the shelter. In the second, we used a machine-based approach using automated extracted movement data from the videos to detect the ERT for each trial (Fig. 3a,b) and used this information to calculate a mean ERT (Fig. 3c). The ERTs calculated using the two different approaches were not significantly different (Extended Data Fig. 2b). We then analyzed the calcium signal from the escape trials and used an algorithm to detect the first time point during stimulus presentation at which the signal was more than two times the median absolute deviation (MAD). This allowed us to detect the first inflection point in the signal that indicates an increase in activity (Fig. 3c). This revealed an increase in the neural signal before the actual deployment of the escape behavior.

Temporally locking the CRH[GCaMP] signal to the ERT in each escape trial (Fig. 3d) revealed a ramping in CRH[PVN] neuron activity during the presentation of the static shadow and before flight initiation (Fig. 3d,e). Once the animal reached the shelter, there was a decrease in the activity of CRH[PVN] neurons (Fig. 3f). These findings indicate that CRH[PVN] neurons generate an anticipatory or preparatory signal before the initiation of an innate escape

response to a descending predator. Inhibition of CRH[PVN] neurons only during the period of ramping activity (the first 5 s of the stimulus presentation) was sufficient to shift the balance of observed innate defensive behaviors in the looming-shadow test (Fig. 3g–i). This preparatory activity during the shadow-expansion phase may signal an increase in threat imminence and facilitate escape behavior[14].

Relationship between CRH[PVN] neuron activity and other innate escape behaviors. This anticipatory or preparatory activity in CRH[PVN] neurons could represent a response specifically to an increase in threat imminence in this specific task or it may be a signature of a more generalizable, but volitional, escape maneuver, or it may simply be indicative of a transition from rest to locomotion. To distinguish between these possibilities, we conducted three different experiments. In the first, we examined CRH[PVN] neuron activity in response to approach and handling by an experimenter (Fig. 4a and Supplementary Fig. 4a). We reasoned that this would mimic the looming shadow but with two important differences: first, no shelter is available for escape; second, the experimenter picks up the mouse, allowing us to test whether the CRH[PVN] neuron response signals a potential escape or codes for a general threat. As in the looming-shadow test, there was an increase in CRH[PVN] neuron activity in response to the advancing hand of an experimenter, and the increase was more evident during the pick up (Fig. 4b). The peak increase observed during the handling manipulation in CRH[PVN] neuron activity was not different to that observed in response to a FS (Supplementary Fig. 4b). Next, we used tail suspension as a model to interrogate the link between CRH[PVN] neuron activity and a volitional escape-type behavior that is not triggered by a visual stimulus or an overt increase in threat imminence. We attached an accelerometer to the fiber housing to obtain high temporal resolution movement data combined with GCaMP signals from CRH[PVN] neurons during a tail suspension experiment (Fig. 4c). The accelerometer detected repeated bouts of activity that relate to putative escape attempts and are consistent with classical descriptions of struggling behavior (Supplementary Fig. 5). Each bout of escape behavior was accompanied by an increase in the activity of CRH[PVN] neurons (Fig. 4d). A closer examination of the data, focusing specifically on the temporal relationship between the CRH[GCaMP] signal and the struggle bout, revealed that CRH[PVN] neuron activity increased before the initiation of a putative escape, which is consistent with a role for these neurons as a preparatory node that is recruited before escape initiation (Fig. 4e,f). Finally, to determine whether CRH[PVN] neuron activity was specific to an escape maneuver or whether it simply reflected an increase in locomotor activity, we analyzed the photometry signal during homecage activity, focusing specifically on transitions from sedentary activity (sitting, sleeping or surveying) to locomotion (Fig. 4g). We did not observe a temporal relation between activity onset and CRH[PVN] neuron activity. These findings demonstrate that CRH[PVN] neurons anticipate motor responses that are volitional and intended to escape threat.

Fig. 3 | CRH[PVN] neurons anticipate the escape response to an imminent threat. a, Example trace of movement analysis during the looming-shadow experiment. a.u., arbitrary units. **b**, Three examples of CRH[PVN] calcium signals (gray) with automated analysis of raw activity trace (blue) and binarized activity trace (orange). **c**, Distribution of the first inflection point in the CRH[GCaMP6] signal after the onset of the stimulus (ERT: 4.8 ± 0.11 s; gray, individual trials; dark blue, Gaussian fit of data) and the escape reaction time (black, individual trials; light blue, Gaussian fit of data). **d**, Average z-score of CRH[PVN] calcium responses with individual trials time-locked to the onset of escape indicated by the dashed line and red arrow ($n = 21$ trials, $N = 5$ mice). **e**, Individual z-score values at baseline (white circles) and onset of escape (blue circles) ($n = 21$ trials, $N = 5$ mice; two-tailed paired t-test, $t(20) = 3.550$, $P = 0.0020$, 95% CI: 0.7449 to 2.868). **f**, Average z-score of CRH[PVN] calcium responses locked at shelter entry (red arrow; $n = 21$ trials, $N = 5$ mice). **g**, Experimental protocol for the CRH[Arch3.0] experiment. Photoinhibition of CRH[PVN] neurons occurred during the first 5 s of stimulus presentation. **h**, Individual trials ($n = 35$ trials, $N = 7$ mice) showing behavior. **i**, Summary of all behaviors in response to CRH[Arch3.0] activation. Behavioral profile (escape, freeze, no response) compared to CRH[eYFP] ($n = 35$ trials, $N = 7$ mice, $\chi^2 = 13.53$, d.f. = 2, $P = 0.0012$). Data compiled and presented as the fraction of trials in each mouse. Solid lines represent the average and shaded areas indicate the s.e.m. Data shown represent the mean $\pm$ s.e.m.

Stress controllability training modifies behavior and alters plasticity at glutamate synapses. In addition to situation-specific shifts in strategy that are due to direct prior experience, rodents show changes in defensive escape behavior following instrumental training in unrelated situations. Specifically, when subjected to aversive training paradigms in which a subject has control over the outcome
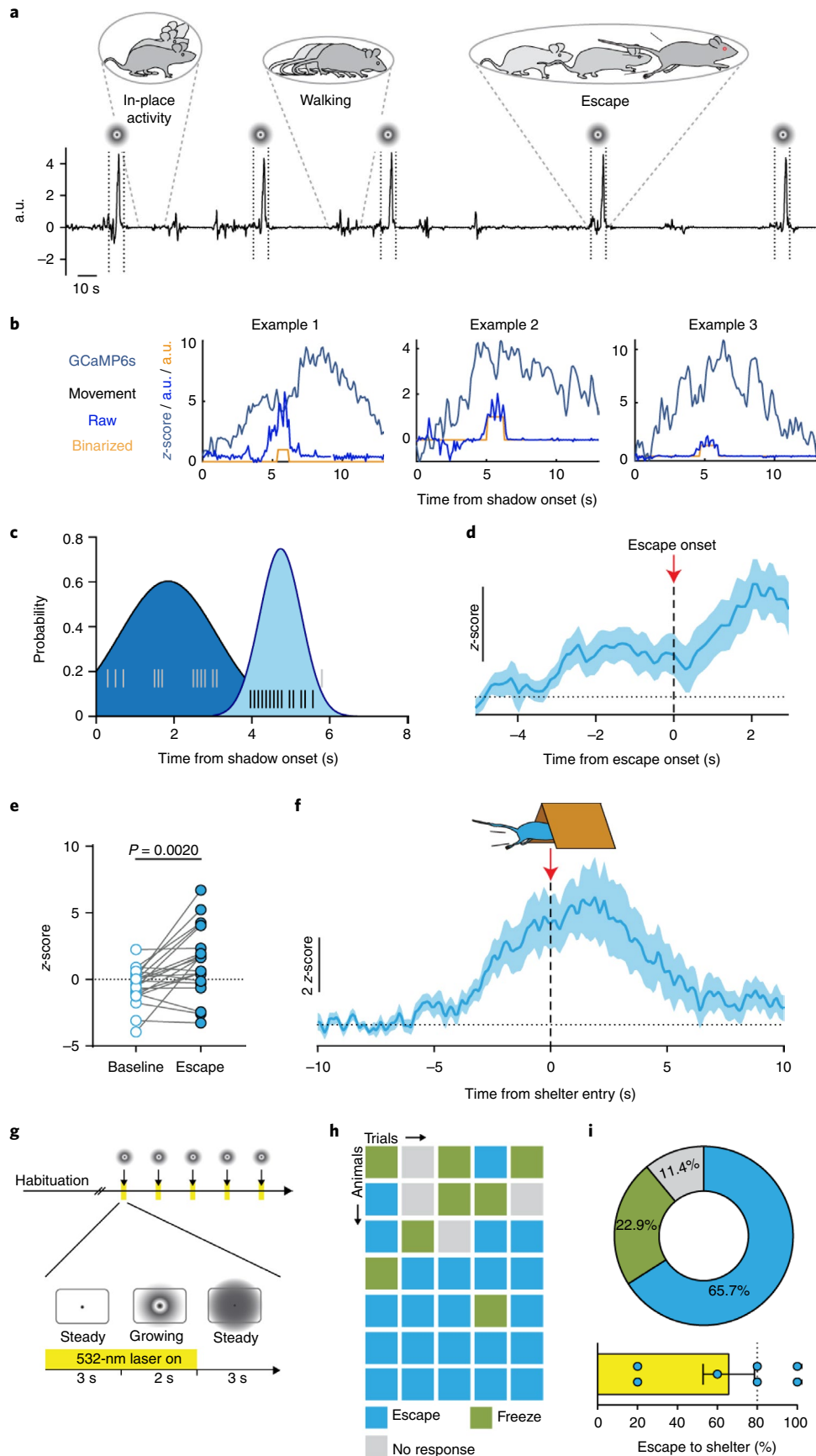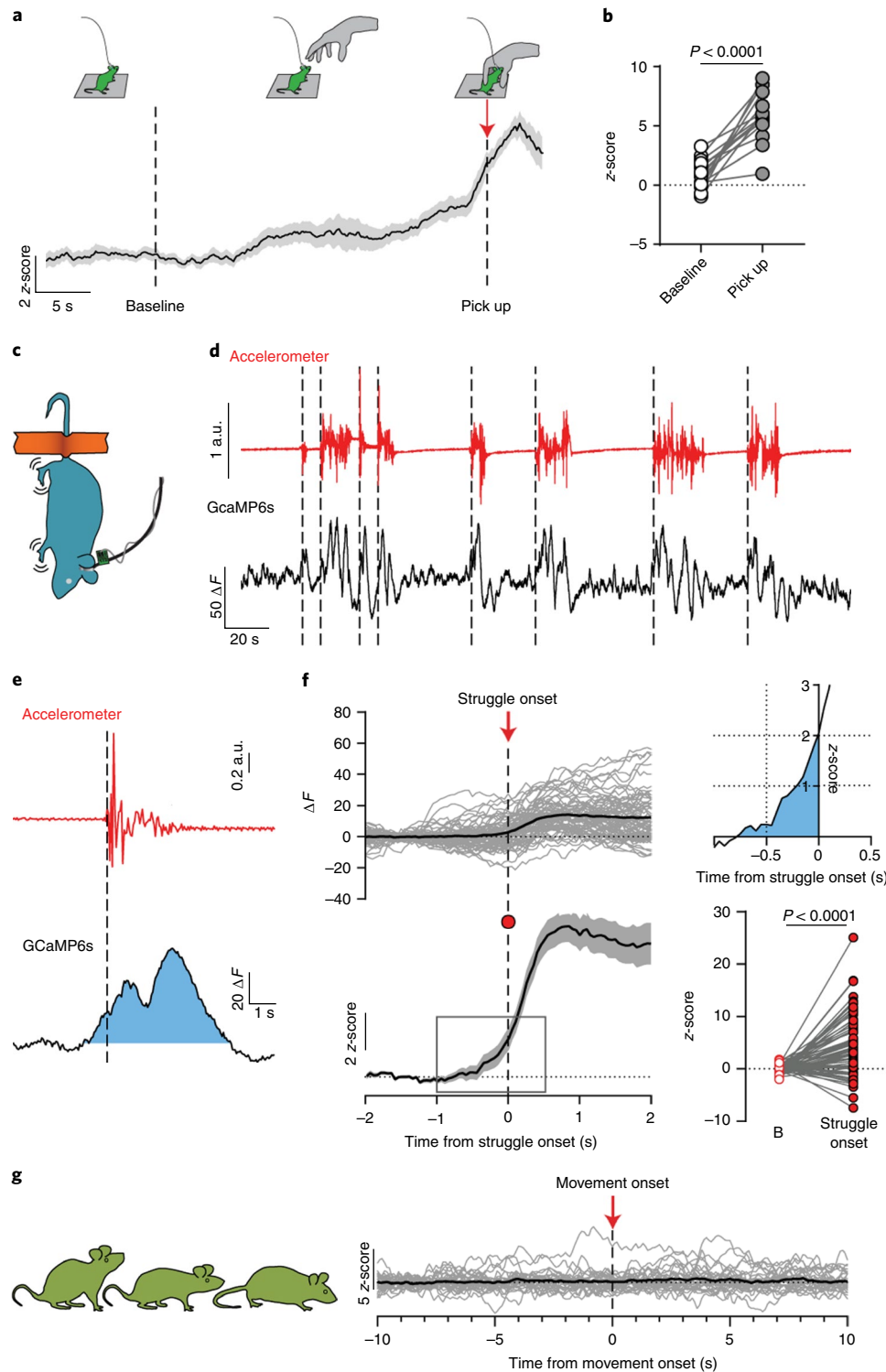
Fig. 4 | Relationship between CRH^PVN neuron activity and other innate escape behaviors. a, Mean trace showing CRH^PVN neuron activity before and during a pick-up maneuver by an experimenter. **b**, Summary of z-scores comparing baseline and time of pick-up (paired t-test, two-tailed, $t(14) = 7.744$, $P < 0.0001$, $N = 15$ mice). **c**, Pictorial representation of the tail-suspension experiment combining single-fiber photometry equipped with an accelerometer. **d**, Example trace of accelerometer (red) and CRH^PVN neuron activity (black) during the tail-suspension experiment. Each dashed line indicates the onset of a struggle bout. **e**, An example of a single bout of struggle, depicting the accelerometer signal and CRH^PVN neuron activity. **f**, Individual traces (gray, top left) and mean (overlaid, black) of CRH^PVN neuron activity, with the average z-score during discrete struggle bouts (bottom left), where $t = 0$ represents the onset of the movement (indicated by the dashed line and red arrow). Magnification of the average z-score locked at the struggle onset (top right), and individual z-score values at the baseline (−1.5 s, open circles) and at the onset of struggle bout (bottom right; filled circles) (two-tailed Wilcoxon signed-rank test, $W = 1925$, $P < 0.0001$; $n = 73$ bouts, $N = 5$ mice). **g**, Individual traces (gray) and average trace (overlaid, black) of CRH^PVN neuron activity during the transition from sitting to moving (transition indicated by the dashed line and red arrow; $n = 31$ trials, $N = 4$ mice). Solid lines represent the average and shaded areas indicate the s.e.m. Summary data shown represent the mean ± s.e.m.

(escape or avoid in response to tone before shock), rodents learn to use the cue to anticipate the shock and initiate escape[3]. Following training, they adopt more active strategies in response to other threats. By contrast, individuals with no control over the outcome (shock is independent of the behavior displayed) adopt passive defensive behaviors during subsequent challenges[4]. Although controllable and uncontrollable stress have similar effects on hypothalamic–pituitary–adrenal output, there is no information about the effects of relative controllability on CRH[PVN] neuron activity or on innate, unlearned defensive behaviors. Here, we used a modified controllability protocol in mice[13] to assess activities of CRH[PVN] neurons and behavior (Fig. 5a). The protocol was a 5-s auditory tone before a 3-s FS in each of two groups of mice. In one group (controllable stress), if the mouse crossed to the opposite side of the shuttle box during the tone presentation (avoid) or FS administration (escape), the shock was terminated. In the other group (uncontrollable stress), there was no instrumental control of the outcome. This group was yoked to the controllable group. Each group was subjected to 20 trials a day for three successive days (Fig. 5b). When we assessed the behavior of the mice during the training protocol, mice in the controllable group showed a consistent increase in shuttling behavior on each of the three successive training days (Fig. 5c and Extended Data Fig. 3). Furthermore, when returned to the training environment on days 2 and 3, mice exposed to controllable and uncontrollable stress showed freezing behavior, but the controllable group spent significantly less time freezing than the uncontrollable group (Fig. 5d). These findings, indicative of a blunted contextual fear response, are consistent with previous work on the consequences of controllable and uncontrollable stress in rat models[19].

Next, we tested whether the two training paradigms had distinct consequences for the intrinsic or synaptic properties of CRH[PVN] neurons. Whole-cell recordings from CRH[PVN] neurons in brain slices did not reveal differences in the intrinsic neuronal excitability between the two groups or in spontaneous synaptic activity (Extended Data Fig. 4). Since we have previously reported[9,20] that acute stress encodes a form of metaplasticity that is unmasked when glutamate synapses are interrogated with tetanic stimuli, we tested whether a similar activity-dependent short-term potentiation following either controllable or uncontrollable stress occurs. Activity-dependent synaptic metaplasticity was evident 24 h after the last training session in the uncontrollable stress group, but not in the controllable stress group (Fig. 5f–h). These changes in the synaptic properties are consistent with a robust recruitment of CRH[PVN] neurons during stress exposure[10].

CRH[PVN] neurons encode stress controllability. Next, we assessed the effects of controllability training directly on the activity of CRH[PVN] neurons in vivo. To establish links between the timing of the protocol, the neuronal response and the behavior, we examined the activity of CRH[PVN] neurons in three distinct time windows: before tone (baseline), during the tone and during tone plus shock (Fig. 6a). Since CRH[PVN] neurons show an increase in activity before an innate escape behavior, we hypothesized that this feature of the activity profile may be discretely affected by controllable versus uncontrollable stress (that is, activity before shock). In both the controllable and uncontrollable groups, there was an increase in the activity of CRH[PVN] neurons to the shock (Fig. 6a and Extended Data Fig. 5a). The absolute peak response to shock was not different between the controllable and uncontrollable groups (Fig. 6b). Consistent with similar peak CRH[PVN] activity signatures, we did not observe differences in circulating corticosterone levels between the two groups (Extended Data Fig. 6).

Next, we analyzed the activity profile during the tone period before the shock. Following 1 day of training, only the controllable group showed an increase in CRH[PVN] neuron activity to the tone (Fig. 6c). This appeared to be an emergent increase in activity over repeated trials (Extended Data Fig. 5c). Following each additional day of training, there was a further increase in this cue-linked response in the controllable group (Fig. 6c–e). By contrast, there was no increase in the anticipatory response of CRH[PVN] neurons in the uncontrollable group (Fig. 6c–e). Plotting the z-scores at the end of the tone phase as distributions revealed a difference between the controllable and uncontrollable groups at the end of 3 days of training (Fig. 6f). This differential increase in anticipatory activity between the controllable and uncontrollable groups was also evident as a decrease in the change in z-score between the onset of shock and the peak CRH[PVN] neuron response in the controllable group, but not in the uncontrollable group (Extended Data Fig. 5b). These observations indicate that controllable and uncontrollable stress paradigms differentially train the activity of CRH[PVN] neurons with predictable shifts in escape behavior. Learned escape is associated with a cue-induced increase in CRH[PVN] neuron activity that occurs before motor action. Meanwhile, when escape is not the likely outcome (the cue does not reliably signal escape), there is no change in the activity of these neurons in response to the FS signaling cue.

To determine whether these activity profiles in the anticipatory phase are a neural signature of the effects of controllable versus uncontrollable stress, we applied an artificial decoder from a Matlab-based massive feature extraction framework to automatically extract quantitative metrics from calcium traces[21]. We subsequently trained a support vector machine with a radial basis function (SVM–RBF) kernal in Matlab using fivefold cross-validation and tested whether this decoder was able to classify the stress-training condition on basis of the activity of CRH[PVN] neurons. We grouped time traces by training day (day 1, day 2, day 3 or all days) and created a labeled raw data matrix with class labels representing the stress-training condition (controllable versus uncontrollable) (Fig. 6g). Based on the calcium signals obtained during the training sessions, the decoder correctly classified (true positives) at a rate of 81% for uncontrollable and 82% for

Fig. 5 | Stress controllability training modifies behavior and alters plasticity at glutamate synapses. a, Stress controllability training protocol depicting the controllable (C) group on the left, in which there is opportunity to escape shock by shuttling to the opposite side of the arena; the uncontrollable (UnC) group is depicted on the right. The behavior of the uncontrollable group has no effect on shock delivery, and shock is determined by the decision of a partner mouse undergoing controllable training. **b**, The training session protocol comprised 3 training days with 20 trials per day. **c**, Left: escape latency for each trial from one mouse in the controllable group. Right: mean escape latency for all mice subjected to controllable stress on a trial-by-trial basis for each training day. Gray column represents the tone period; yellow represents the tone and shock ($N = 6$ mice for each group). **d**, Freezing behavior in the conditioned context before daily training (day 1 to day 3, $N = 10$ mice for each group). Two-way repeated-measures ANOVA, group factor $F_{(2,36)} = 40.86$, $P < 0.001$. Day 1: $P > 0.9999$, 95% CI: −9.253 to 10.47. Day 2: $P < 0.0001$, 95% CI: 13.51 to 33.23. Day 3: $P = 0.0473$, 95% CI: 0.0896 to 19.81. **e**, Schematic depiction of whole-cell patch-clamp recordings from CRH[PVN] neurons. **f**, Representative traces of EPSCs before and after a 100 Hz high-frequency stimulation (HFS) delivered to afferent fibers synapsing on CRH neurons. **g**, Summary of EPSC amplitudes following HFS (gray bar) relative to baseline from controllable group (mean: 114.5 ± 9.5, $n = 25$ cells, $N = 9$ mice, Wilcoxon signed-rank test, two-tailed $W = 99.00$, $P = 0.1908$ versus baseline) and uncontrollable mice (mean: 147.4 ± 11.4, $n = 31$ cells, $N = 10$ mice, Wilcoxon signed-rank test, two-tailed, $W = 416$, $P < 0.0001$ versus baseline). **h**, Individual data representing the EPSC amplitude 1 min after HFS in each group (controllable: $N = 9$ mice, $n = 25$ cells; uncontrollable: $N = 10$ mice, $n = 31$ cells; Mann–Whitney test, two-tailed, $U = 251$, $P = 0.0242$). Summary data shown represent the mean ± s.e.m.

controllable (Fig. 6h,j) when trained and tested with data pooled from all 3 days of training. In addition, when applied to traces from each day separately, the classifier was better at discriminating between controllable and uncontrollable stress on the third day of training than the first day of training (Fig. 6i and Extended Data Fig. 7). This analysis indicates that the features in the calcium signal obtained from CRH[PVN] neurons following controllable and uncontrollable training are distinct from each other and

can predict, with >80% accuracy, the stress protocol that the subject had experienced.

Controllability alters responses to cue and shadow to result in a biased defensive strategy. Since anticipatory CRH[PVN] neuron activity increases before escape behavior in other tasks, we tested whether changes in this activity as a consequence of behavioral training would generalize to the looming-shadow task and modify
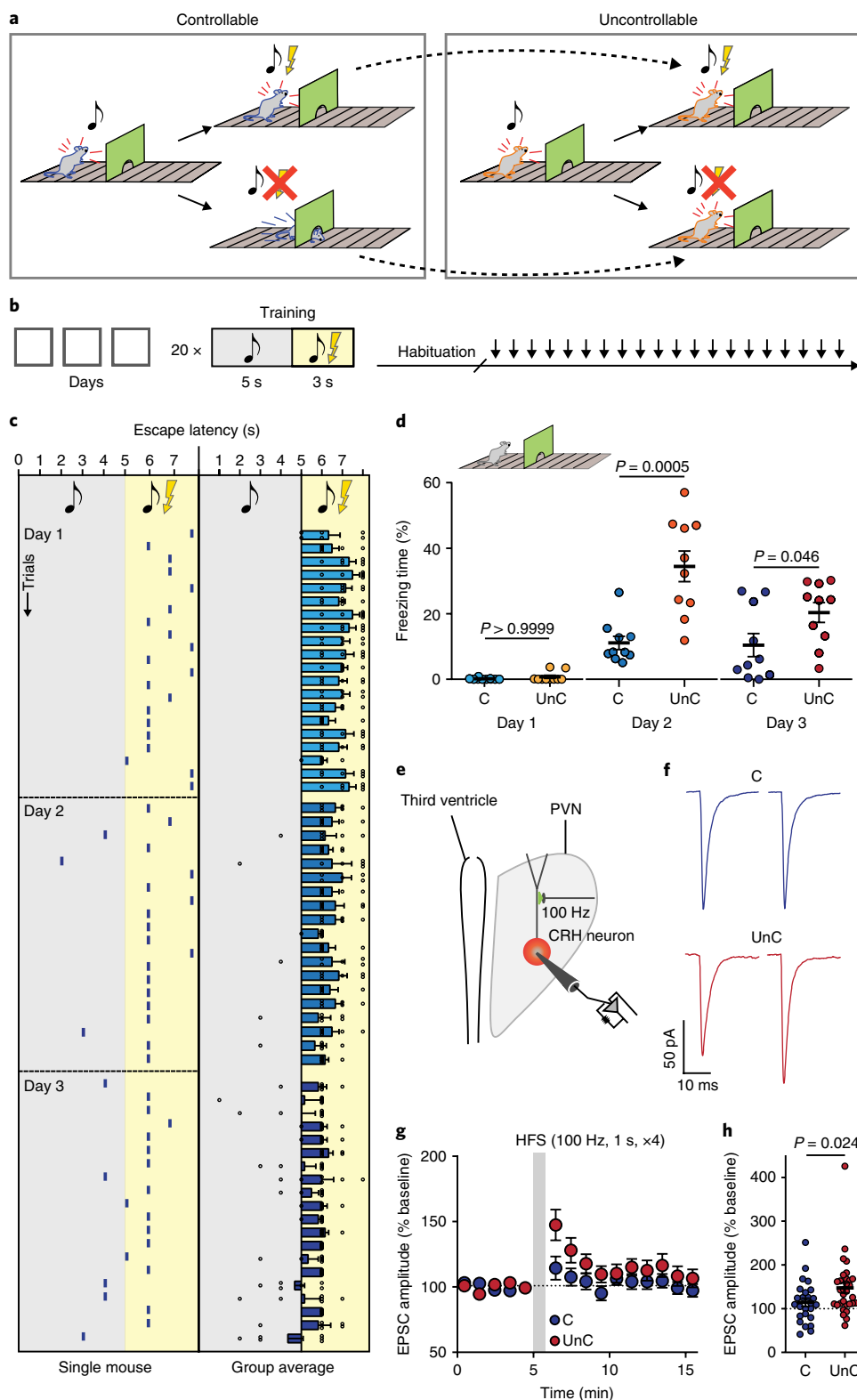
defensive behavior. First, we tested whether the activity signature imparted by training could be recalled by CRH^{PVN} neurons even if the context was altered. Forty-eight hours after the last training session, mice were placed in a novel arena and the tone used in training was delivered (Fig. 7a and Extended Data Fig. 8). There was an increase in CRH^{PVN} neuron activity to the tone in mice subjected to controllable stress (Fig. 7b, left), but not in mice subjected to uncontrollable stress (Fig. 7b, right). Since CRH^{PVN} neurons continue to show divergent responses to cue after training, we asked whether this would generalize 1 week later and affect behaviors in the looming-shadow paradigm. Mice subjected to controllable stress showed an anticipatory increase in the activity of CRH^{PVN} neurons (Fig. 7c, left). By contrast, mice subjected to uncontrollable stress failed to show anticipatory responses to the shadow (Fig. 7c, right). CRH^{PVN} neuron activity at the end of the expansion phase of the shadow (5 s) was higher in the controllable group compared with the uncontrollable group, which is consistent with an anticipatory increase in activity before the escape behavior (Fig. 7d). The higher CRH^{PVN} neuron activity in the controllable group during the expansion

phase of the stimulus was followed by escape behavior in 96% of the trials (Fig. 7e, left). The uncontrollable group showed a decrease in escape probability (Fig. 7e, right; uncontrollable $P_{escape} = 0.40$

Fig. 6 | CRH^{PVN} neurons encode stress controllability. a, Left three panels show individual (gray) and mean (blue) calcium traces for controllable group; right three panels show individual (gray) and mean (orange) calcium traces for uncontrollable group. The baseline period is the leftward white column; the tone is represented as the gray column and the tone plus FS is shown as yellow. Day 1: controllable: $n = 120$ trials, $N = 6$ mice; uncontrollable: $n = 120$ trials, $N = 6$ mice. Day 2: controllable: $n = 114$ trials, $N = 6$ mice; uncontrollable: $n = 119$ trials, $N = 6$ mice. Day 3: controllable: $n = 120$ trials, $N = 6$ mice; uncontrollable: $n = 120$ trials, $N = 6$ mice. **b**, Individual z-score values at the peak of the FS (peak) response for each stress training group (day 1: Mann–Whitney test, two-tailed, $U = 6,445$, $P = 0.1606$; day 2: Mann–Whitney test, two-tailed, $U = 5,367$, $P = 0.1046$; day 3: Mann–Whitney test, two-tailed, $U = 6,642$, $P = 0.7028$). Day 1: controllable: $n = 120$ trials, $N = 6$; uncontrollable: $n = 120$ trials, $N = 6$ mice. Day 2: controllable: $n = 114$ trials, $N = 6$ mice; uncontrollable: $n = 119$ trials, $N = 6$ mice. Day 3: controllable: $n = 120$ trials, $N = 6$ mice; uncontrollable: $n = 120$ trials, $N = 6$ mice. **c**, Average z-score for each day of training for controllable (left three panels, blue) and uncontrollable (right three panels, orange) during 5 s of baseline (white column) and 5 s of tone presentation (gray column) (top, day 1, middle, day 2 and bottom, day 3) ($n = 120$ trials per day, $N = 6$ mice per group). **d**, Quantification of z-scores at the end of the tone phase before shock for day 1 (top; Mann–Whitney test, two-tailed, $U = 5,807$, $P = 0.0096$), day 2 (middle; Mann–Whitney test, two-tailed, $U = 3,679$, $P < 0.0001$) and day 3 (bottom; Mann–Whitney test, two-tailed, $U = 4,200$, $P < 0.0001$) for both controllable and uncontrollable groups. Day 1: controllable $n = 120$ trials, $N = 6$ mice; uncontrollable: $n = 120$ trials, $N = 6$ mice. Day 2: controllable: $n = 114$ trials, $N = 6$ mice; uncontrollable: $n = 119$ trials, $N = 6$ mice. Day 3: controllable: $n = 120$ trials, $N = 6$; uncontrollable: $n = 120$ trials, $N = 6$ mice. **e**, Cumulative distributions of z-scores at the end of the tone phase (5 s) for day 1 versus day 3 in both controllable (top, blue) and uncontrollable (bottom, orange). **f**, Cumulative distributions of z-scores at the end of tone alone phase (5 s) for controllable (blue line) versus uncontrollable (orange line) on day 1 (top) and day 3 (bottom). **g**, Example of the time-series database used for the classifier training; controllable (blue), uncontrollable (orange). **h**, Confusion matrix showing the classification accuracy (ratio of correct predictions to total predictions made) of the trained decoder using all training days in the model. **i**, Linear regression ($R^2 = 0.9643$) showing the increase in accuracy of the classifier when trained using individual training days (day 1 = 67.5%, day 2 = 75.5%, day 3 = 79.5%) **j**, The receiver operating characteristic (ROC) curve illustrating the discrimination index for both controllable (left) and uncontrollable (right) group in a binary classifier. Red circle represents current classifier. AUC, area under the curve. Solid lines represent the average and the shaded areas indicate the s.e.m. Data shown represent the mean ± s.e.m.
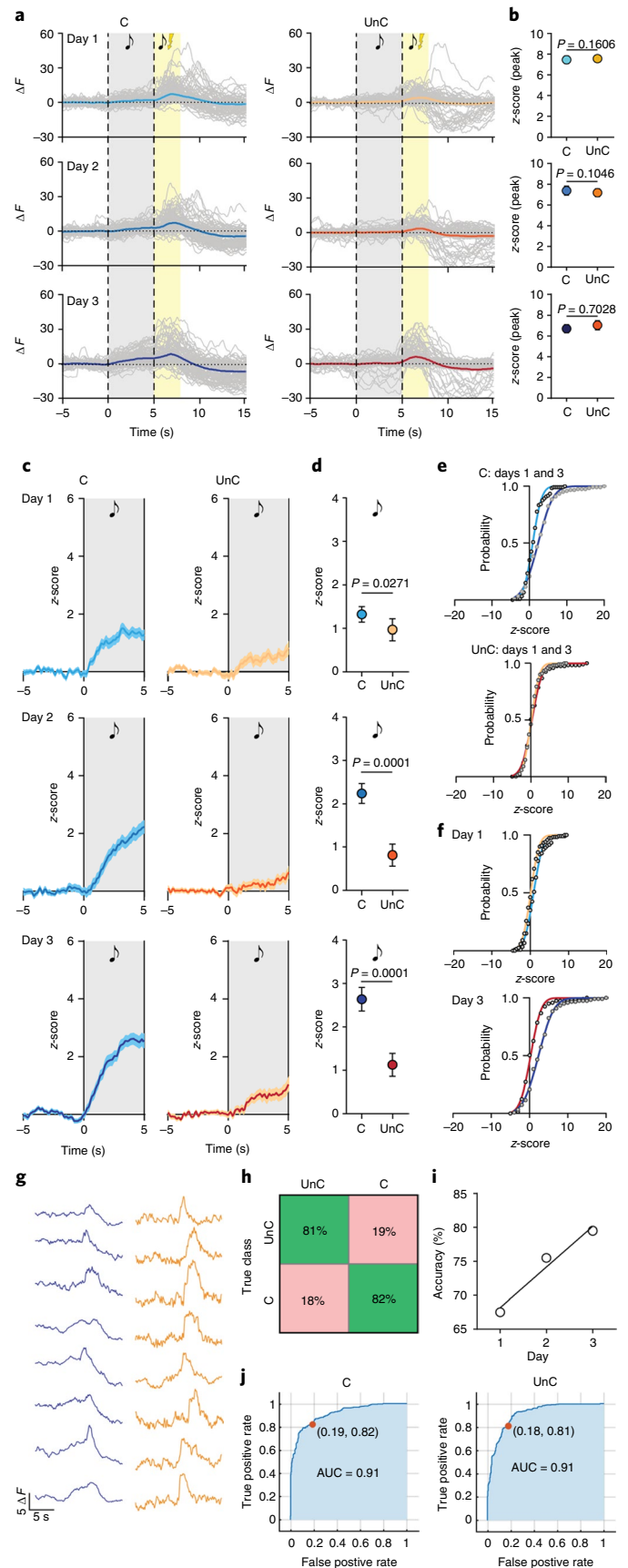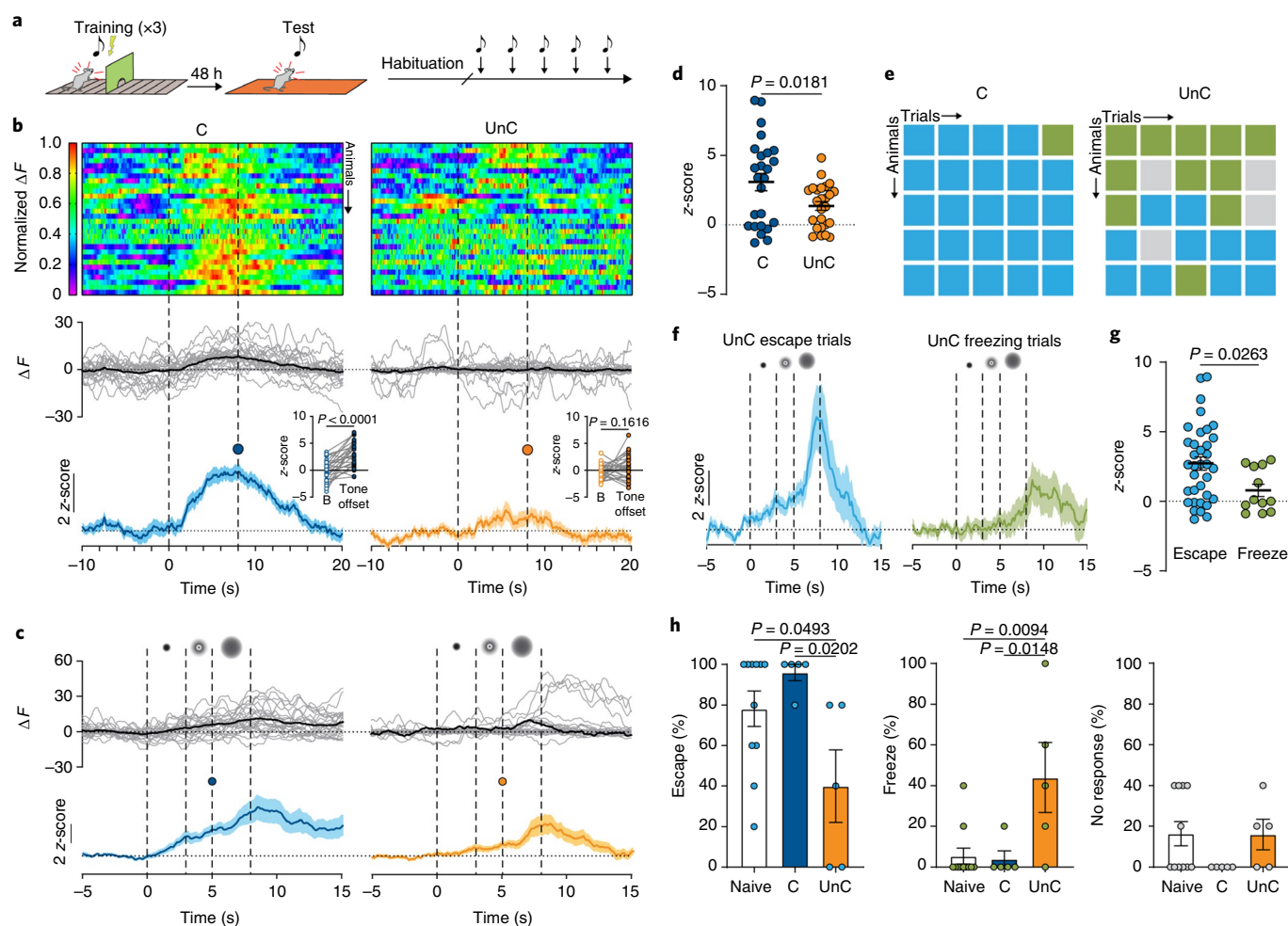
Fig. 7 | Controllability training shifts the defensive strategy. a, Protocol of conditioned tone exposure 48 h after the last day of training. **b**, Top: heatmaps of normalized ΔF calcium responses of individual trials for controllable and uncontrollable groups in response to conditioned tone response ($n = 30$ trials, $N = 6$ mice for each group). Middle: individual (gray) and mean (overlaid black) calcium traces for controllable (left) and uncontrollable group (right) during conditioned tone presentation. Bottom: average z-score of CRH^{PVN} calcium response during tone presentation for controllable (left, blue) and uncontrollable (right, orange) groups. Inset: average z-score of CRH^{PVN} calcium response and quantification of z-score at the onset (white circles) and offset (filled circles) of tone presentation for controllable (left, blue circles: paired t-test, two-tailed, $t(30) = 5.960$, $P < 0.0001$, 95% CI: 1.921 to 3.927) and uncontrollable (right, orange circles: paired t-test, two-tailed, $t(30) = 1.437$, $P = 0.1616$, 95% CI: −0.3047 to 1.743). Dotted vertical lines represent 8-s duration of tone presentation. **c**, Top: individual (gray) and mean (overlaid black) calcium traces for controllable group (left) and uncontrollable group (right) during the looming shadow test. Dotted vertical lines denote the three phases of the visual stimulus, static dot for 3 s, growing phase for 2 s followed by static phase for 3 s ($n = 25$ trials, $N = 5$ mice for each group). **d**, Average z-score of CRH^{PVN} calcium response at the end of the expansion phase of the visual stimulus for both controllable ($n = 25$ trials, $N = 5$ mice) and uncontrollable ($n = 25$ trials, $N = 5$ mice) (unpaired t-test, two-tailed, $t(48) = 2.447$, $P = 0.0181$). **e**, Individual trials showing behavior during looming-shadow experiment ($n = 25$ trials, $N = 5$ mice for each group). **f**, The uncontrollable group was divided into escapers and freezers, and the average z-score of CRH^{PVN} calcium response is shown (left, blue: escapers $n = 10$ trials, $N = 3$ mice; right, green: freezers $n = 11$ trials, $N = 4$ mice). **g**, Average z-score of CRH^{PVN} calcium response at the end of the expansion phase of the visual stimulus for all escape ($n = 34$ trials, $N = 8$ mice) and all freeze ($n = 12$ trials, $N = 5$ mice) responses (unpaired t-test, two-tailed, $t(45) = 2.345$, $P = 0.0236$, 95% CI: 0.2797 to 3.705). **h**, Data compiled and presented as fraction of trials in each mouse in three different groups: naive ($N = 11$ mice), controllable ($N = 5$ mice) and uncontrollable ($N = 5$ mice). Each behavioral output is represented. Uncontrollable group shows a decrease in escape (one-way ANOVA $F(2,18) = 5.002$, $P = 0.0187$, Holm–Sidak correction), an increase in freezing (one-way ANOVA $F(2,18) = 6.599$, $P = 0.0071$, Holm–Sidak correction), and no difference in the non-responders (one-way ANOVA $F(2,18) = 1.821$, $P = 0.1905$, Holm–Sidak correction). Solid lines represent the average and shaded areas indicate the s.e.m. Data shown represent the mean ± s.e.m.

versus controllable $P_{escape} = 0.90$; Fisher's exact test, $P < 0.0001$). Further analysis of the uncontrollable CRH^{GCaMP} signal specifically revealed different activity profiles in trials resulting in an escape response versus those in which freezing behavior was identified (Fig. 7f; for the no-response group, see Extended Data Fig. 9). In trials resulting in an escape maneuver, the CRH^{PVN} neuron activity at the end of the expansion phase of the stimulus (5 s) was significantly higher than the activity observed in the trials that resulted in a

freezing response (Fig. 7g). Similar to observations in naive mice, the increase in activity of CRH^{PVN} neurons preceded the escape maneuver (Extended Data Fig. 9). When trials across all groups (naive, uncontrollable and controllable) were compiled into either escape or freeze, there was a clear distinction in the anticipatory response of CRH^{PVN} neurons during the phase before escape onset (Extended Data Fig. 10). The increase in freezing behavior and decrease in escape behavior in comparison to naive mice (Fig. 7h) is consistent

with data from the experiments using CRH[Arch3.0] mice. Collectively, these observations demonstrate that controllability training modifies anticipatory activity in CRH[PVN] neurons and results in a shift in defensive strategy in a different, unrelated challenge.

Discussion

Survival is predicated on the detection and avoidance of threat. Since threat is multifaceted, this requires organisms to have access to a palette of innate behaviors designed to evade danger. Under these conditions, the optimal behavior is one that decreases the probability of harm. Since this could be one of many behaviors, organisms use prior experience to optimize the decision-making process. When organisms cannot rely on prior experiences, they choose from a palette of innate behaviors that has been honed through evolutionary pressure.

In response to the looming-shadow procedure, which mimics an advancing threat from the sky, the balance between active and passive strategies appears to be hardwired toward active escape behavior. In all naive groups (Crh-IRES-Cre, CRH[GCaMP] and CRH[eYFP]), we consistently observed an escape probability of approximately 80% (range of 78.5–84%). Our data support the ideas on a hierarchical organization of defensive behavior in rodents[22]. According to this framework, freezing is the dominant behavior in response to a potential threat that remains distant, but as the threat advances and there is the possibility that escape offers a favorable outcome (shelter is available), then escape becomes the dominant behavior. Our data are consistent with this idea; that is, an increase in threat imminence, combined with an opportunity, forces a shift in the behavioral strategy to active escape behavior. However, future experiments in which the imminence of the threat stimulus is systematically varied will be required to directly confirm this idea. This increase in escape probability requires an increase in the activity of CRH[PVN] neurons when the threat is advancing. Furthermore, we demonstrated that controllability training, by altering the activity of CRH neurons, shifts defensive strategies in subsequent, unrelated situations that signal danger.

CRH[PVN] neurons anticipate escape behavior. We demonstrated that CRH[PVN] neuron activation anticipates, or occurs before, the initiation of an escape behavior. This occurred in response to a looming advancing shadow and in a tail-suspension protocol in which the animal struggles to escape. By contrast, this anticipatory activity was absent during a passive defensive behavior such as freezing, thereby providing a correlation between the activity of these cells and the choice of an active defensive behavior. This link was further strengthened by the observation that optogenetic silencing of CRH[PVN] neurons, either during the full procedure or coincident with the timing of the ramping activity, resulted in a shift toward a more passive defensive strategy. This switch in strategy indicates that CRH[PVN] neurons are key players in unlearned escape initiation. The switch between defensive strategies has also been linked to activity changes in somatostatin neurons in the central amygdala[18], which suggests that multiple nodes are critical for the choice of defensive behavioral strategy. It is important to highlight that our study focused on natural flight behavior that requires no learning and that a careful comparative dissection of circuits for learned and unlearned flight behaviors has not been done. Our finding that CRH[PVN] neurons also increase their activity before the onset of struggling in the tail-suspension test suggests that these may play a key role in active defensive behaviors. Interestingly, prior exposure to the looming-shadow paradigm also resulted in a strategy switch; in this case, instead of freezing, animals did not show overt defensive behavior. We hypothesize that this may be due to the fact that the first exposure to the paradigm itself had no direct consequence for the animal.

By using a model that takes advantage of the fact that rodents in the wild experience danger that often comes from above (flying predators)[14], we were able to demonstrate that CRH[PVN] neurons participate in the initiation of active defensive behaviors to a visual threat. This positions these cells as part of circuit that includes retinal ganglion cells[20], parvalbumin excitatory projection neurons in the superior colliculus[23], the medial superior colliculus and the dorsal periaqueductal gray[24], the basolateral amygdala[25] and the dorsal raphe nucleus[26]. This is, to the best of our knowledge, the first description linking CRH[PVN] neurons to innate defensive behavior in response to visual threat. In addition to the nuclei described above, the ventromedial hypothalamus, which projects to the PVN, has been implicated in defensive behavior[27]. An additional and intriguing, but unexplored, possibility is through direct projection from the retina to the PVN, which has been described in rodents, hamsters and humans[28,29]. The time lag between an increase in activity and initiation of escape suggests that the neurons may not drive the motor response per se, but may instead contribute to the preparation of multiple systems before the initiation of escape. Indeed, their position adjacent to autonomic output cells in the PVN, combined with observations that electrical stimulation of the PVN increases blood flow to the hindlimb of rats[30], is consistent with a potential preparatory role that coordinates sympathetic output before initiation of a flight response. It is widely accepted that for a given motor action, a synchronized activity of distributed neuronal populations is needed[31]; here, we showed a new role for CRH[PVN] neurons before escape initiation. Our findings, together with observations in zebrafish linking activation of the hypothalamic corticotropin system with rapid locomotive behavior and stressor avoidance[10], hint at an evolutionarily conserved role for this cell population in escape initiation. Future experiments are required to establish the mechanisms through which this 'pre-action' state can be manipulated.

CRH[PVN] neurons encode controllability. Although CRH[PVN] neurons are essential for the endocrine response to stress, their role in stress controllability has not been well studied. Stress-induced changes in *CRH* mRNA levels in the PVN[32] and endocrine and autonomic responses[4,12] are similar in controllable and uncontrollable groups. Consistent with these data, we showed that the peak activity of CRH[PVN] neurons and the levels of circulating corticosterone were indistinguishable in controllable and uncontrollable stress. Our data did, however, provide support for the hypothesis that CRH[PVN] neurons encode information that is distinct in the controllable versus uncontrollable stress paradigms. Specifically, we observed an increase in the anticipatory response to cue before delivery of the aversive shock during the course of controllable training; by contrast, the anticipatory activity was unchanged by uncontrollable stress training. When we provided these activity signatures, even in the absence of information about the training protocol, to a machine decoder, it was able to successfully declassify the training condition. This suggests that this anticipatory activity signature is an important feature that may allow CRH neurons to decode prior experiences with different levels of relative controllability.

Linking changes in CRH[PVN] neuron activity and innate survival behaviors. Others have shown that the perception of control during an aversive event can also have long-term consequences for behavioral choice[33,34]. The perception of control in one task has been linked to increased active or escape-like behavior during subsequent tests. By contrast, the perception of little or no control during an aversive event has been linked to increased passive or freezing behavior or indifference. We showed an unexpected role for CRH[PVN] neurons in translating controllability to a behavioral outcome. Our data indicated that control over the outcome in one situation increased anticipatory activity of CRH[PVN] neurons before the initiation of an escape behavior in a different situation.

Specifically, CRH[PVN] neurons showed ramping in their activity in response to an auditory cue that is an associative predictor of a FS. This anticipatory response was accompanied by an increase in escape or avoid responses. Furthermore, the ability of CRH[PVN] neurons to respond to the cue alone even days after the termination of the controllable training provides clear evidence that these cells retain information linked to signals that predict an aversive stimulus. This increase in anticipatory activity resulted in a more responsive system when other threats, even those that were completely novel, were presented. The behavioral outcome was an increase in active escape responses. Conversely, the absence of control dampened the anticipatory response to cues that may signal threat, resulting in a decrease in active responses during other challenges. This suggests that uncontrollable training, by blunting anticipatory activity during cue presentation, effectively degrades the link between the stimulus and the action.

Although we did not specifically examine valence coding in our study, this is an important consideration given that CRH[PVN] neurons respond to negative valence[11]. Our data from the FS exposure are consistent with findings that CRH[PVN] neurons are key mediators of rapid sensory detection of aversive stimuli[11]. CRH[PVN] neurons in both the controllable and uncontrollable groups responded during the aversive stimulus itself, but the anticipatory response to the cue that predicts the shock appeared to show an inverted relationship to valence. If CRH[PVN] neurons were simply negative valence responders, then there should be a robust increase in activity in response to the tone alone in the uncontrollable group. Instead, we did not see any anticipatory activity of CRH[PVN] neurons in mice subjected to uncontrollable training or an increase in activity during controllable training. Although these observations argue against negative valence coding, additional experiments will be required to directly address this notion.

Until now, relatively little has been known about how stress controllability can generalize to modify behaviors in different situations. Although there is compelling information about the role of the medial prefrontal cortex in regulating the activity of dorsal raphe neurons in controllable stress paradigms to modify subsequent learned behaviors[35], little is known about stress control and innate defensive behaviors. Understanding this link is critical, as challenges arise spontaneously and unpredictably, triggering innate defensive behaviors in individuals. Interestingly, innate and learned responses to threat appear to be regulated by different neural networks[36]. Unlearned fear does not require the medial prefrontal cortex (prelimbic)[37]. Our observations indicate that CRH[PVN] neurons are an intersectional node for innate and learned defensive behaviors. By exploiting this feature, we were able to train CRH[PVN] neurons to increase or decrease their activity in one situation and as a result modify behavioral output.

In humans, there is strong evidence to indicate that trauma can result in more passive responses or the emergence of learned helplessness during subsequent challenges[38]. We would argue that decreased anticipatory activation of CRH[PVN] neurons, and specifically an inability to engage to specific, predictive cues that should trigger this anticipatory activity, may contribute to this learned helplessness. Recent human studies have shown that rapid escape decisions do not rely on cortical regions related to 'cognitive fear' but instead rely on the amygdala, midbrain and hypothalamus that are linked to 'reactive fear'[39]. Importantly, our findings also indicate that this system is trainable and that this type of control training may be useful in a prophylactic fashion to enhance resilient behavior following traumatic events.

Online content

Any methods, additional references, Nature Research reporting summaries, source data, extended data, supplementary information, acknowledgements, peer review information; details of author

contributions and competing interests; and statements of data and code availability are available at https://doi.org/10.1038/s41593-020-0591-0.

References

1. Kushner, M. G., Riggs, D. S., Foa, E. B. & Miller, S. M. Perceived controllability and the development of posttraumatic stress disorder (PTSD) in crime victims. *Behav. Res. Ther.* **31**, 105–110 (1993).
2. Hartley, C. A., Gorun, A., Reddan, M. C., Ramirez, F. & Phelps, E. A. Stressor controllability modulates fear extinction in humans. *Neurobiol. Learn. Mem.* **113**, 149–156 (2014).
3. Maier, S. F. & Watkins, L. R. Stressor controllability and learned helplessness: the roles of the dorsal raphe nucleus, serotonin, and corticotropin-releasing factor. *Neurosci. Biobehav. Rev.* **29**, 829–841 (2005).
4. Maier, S. F. Behavioral control blunts reactions to contemporaneous and future adverse events: medial prefrontal cortex plasticity and a corticostriatal network. *Neurobiol. Stress* **1**, 12–22 (2014).
5. Boeke, E. A., Moscarello, J. M., LeDoux, J. E., Phelps, E. A. & Hartley, C. A. Active avoidance: neural mechanisms and attenuation of Pavlovian conditioned responding. *J. Neurosci.* **37**, 4808–4818 (2007).
6. Füzesi, T., Daviu, N., Wamsteeker Cusulin, J. I., Bonin, R. P. & Bains, J. S. Hypothalamic CRH neurons orchestrate complex behaviours after stress. *Nat. Commun.* **7**, 11937 (2016).
7. Zhang, R. et al. Loss of hypothalamic corticotropin-releasing hormone markedly reduces anxiety behaviors in mice. *Mol. Psychiatry* **22**, 733–744 (2017).
8. Ramot, A. et al. Hypothalamic CRFR1 is essential for HPA axis regulation following chronic stress. *Nat. Neurosci.* **20**, 385–388 (2017).
9. Sterley, T.-L. et al. Social transmission and buffering of synaptic changes after stress. *Nat. Neurosci.* **21**, 393–403 (2018).
10. De Marco, R. J., Thiemann, T., Groneberg, A. H., Herget, U. & Ryu, S. Optogenetically enhanced pituitary corticotroph cell activity post-stress onset causes rapid organizing effects on behaviour. *Nat. Commun.* **7**, 2620 (2016).
11. Kim, J. et al. Rapid, biphasic CRF neuronal responses encode positive and negative valence. *Nat. Neurosci.* **22**, 576–585 (2019).
12. Maier, S. F., Ryan, S. M., Barksdale, C. M. & Kalin, N. H. Stressor controllability and the pituitary–adrenal system. *Behav. Neurosci.* **100**, 669–674 (1986).
13. Liu, X., Tang, X. & Sanford, L. D. Stressor controllability and Fos expression in stress regulatory regions in mice. *Physiol. Behav.* **97**, 321–326 (2009).
14. Yilmaz, M. & Meister, M. Rapid innate defensive responses of mice to looming visual stimuli. *Curr. Biol.* **23**, 2011–2015 (2013).
15. Chow, B. Y. et al. High-performance genetically targetable optical neural silencing by light-driven proton pumps. *Nature* **463**, 98–102 (2010).
16. Cui, G. et al. Deep brain optical measurements of cell type-specific neural activity in behaving mice. *Nat. Protoc.* **9**, 1213–1228 (2014).
17. Gunaydin, L. A. et al. Natural neural projection dynamics underlying social behavior. *Cell* **157**, 1535–1551 (2014).
18. Fadok, J. P. et al. A competitive inhibitory circuit for selection of active and passive fear responses. *Nature* **542**, 96–100 (2017).
19. Baratta, M. V. et al. Controllable versus uncontrollable stressors bi-directionally modulate conditioned but not innate fear. *Neuroscience* **8**, 1495–1503 (2007).
20. Kuzmiski, J. B., Marty, V., Baimoukhametova, D. V. & Bains, J. S. Stress-induced priming of glutamate synapses unmasks associative short-term plasticity. *Nat. Neurosci.* **13**, 1257–1264 (2010).
21. Fulcher, B. D. & Jones, N. S. hctsa: a computational framework for automated time-series phenotyping using massive feature extraction. *Cell Syst.* **5**, 527–531.e3 (2017).
22. Blanchard, R. J., Flannelly, K. J. & Blanchard, D. C. Defensive behaviors of laboratory and wild *Rattus norvegicus*. *J. Comp. Psychol.* **100**, 101–107 (1986).
23. Shang, C. et al. A parvalbumin-positive excitatory visual pathway to trigger fear responses in mice. *Science* **348**, 1472–1477 (2015).
24. Evans, D. A. et al. A synaptic threshold mechanism for computing escape decisions. *Nature* **558**, 590–594 (2018).
25. Hu, Y. et al. A translational study on looming-evoked defensive response and the underlying subcortical pathway in autism. *Sci. Rep.* **7**, 14755 (2017).
26. Huang, L. et al. A retinoraphe projection regulates serotonergic activity and looming-evoked defensive behaviour. *Nat. Commun.* **8**, 14908 (2017).
27. Wang, L., Chen, I. Z. & Lin, D. Collateral pathways from the ventromedial hypothalamus mediate defensive behaviors. *Neuron* **85**, 1344–1358 (2015).
28. Youngstrom, T. G., Weiss, M. L. & Nunez, A. A. Retinofugal projections to the hypothalamus, anterior thalamus and basal forebrain in hamsters. *Brain Res. Bull.* **26**, 403–411 (1991).

29. Schaechter, J. D. & Sadun, A. A. A second hypothalamic nucleus receiving retinal input in man: the paraventricular nucleus. *Brain Res.* **340**, 243–250 (1985).

30. Porter, J. P. & Brody, M. J. Neural projections from paraventricular nucleus that subserve vasomotor functions. *Am. J. Physiol.* **248**, R271–R281 (1985).

31. Feldman Barrett, L. & Finlay, B. L. Concepts, goals and the control of survival-related behaviors. *Curr. Opin. Behav. Sci.* **24**, 172–179 (2018).

32. Helmreich et al. The effect of stressor controllability on stress-induced neuropeptide mRNA expression within the paraventricular nucleus of the hypothalamus. *J. Neuroendocrinol.* **11**, 121–128 (2001).

33. Lucas, M. et al. Long-term effects of controllability or the lack of it on coping abilities and stress resilience in the rat. *Stress* **17**, 423–430 (2014).

34. Maier, S. F. Role of fear in mediating shuttle escape learning deficit produced by inescapable shock. *J. Exp. Psychol. Anim. Behav. Process* **16**, 137–149 (1990).

35. Amat, J. et al. Medial prefrontal cortex determines how stressor controllability affects behavior and dorsal raphe nucleus. *Nat. Neurosci.* **8**, 365–371 (2005).

36. Gross, C. T. & Canteras, N. S. The many paths to fear. *Nat. Rev. Neurosci.* **13**, 651–658 (2012).

37. Corcoran, K. A. & Quirk, G. J. Activity in prelimbic cortex is necessary for the expression of learned, but not innate, fears. *J. Neurosci.* **27**, 840–844 (2012).

38. Nicholson, A. A. et al. Dynamic causal modeling in PTSD and its dissociative subtype: bottom-up versus top-down processing within fear and emotion regulation circuitry. *Hum. Brain Mapp.* **38**, 5551–5561 (2017).

39. Qi, S. et al. How cognitive and reactive fear circuits optimize escape decisions in humans. *Proc. Natl Acad. Sci. USA* **115**, 3186–3191 (2018).

Methods

Mice. All animal protocols were approved by the University of Calgary Animal Care and Use Committee. For behavioral experiments requiring naive mice in the looming-shadow test, C57BL/6-Elite male mice were obtained from Charles River (6–8 weeks old). For fiber photometry (male and female) and stress controllability training (male) Crh-IRES-Cre; Ai14 mice in which CRH neurons express the tdTomato fluorophore were used. These have previously been characterized[40]. Mice were housed on a 12-h light–dark cycle (lights on at 6:00) in whole litters until 1–2 days before use, then were individually housed during the experimental phase. All subjects were randomly assigned to different experimental conditions used in this study. Mice were 6–8 weeks old at the time of surgery and virus injection.

Ex vivo electrophysiology. *Slice preparation.* Twenty-four hours after the last training session, the mice were anesthetized with isoflurane and decapitated. Brains were rapidly removed and immersed in ice-cold slicing solution containing (in mM) 87 NaCl, 2.5 KCl, 0.5 CaCl$_2$, 7 MgCl$_2$, 25 NaHCO$_3$, 25 D-glucose, 1.25 NaH$_2$PO$_4$ and 75 sucrose, saturated with 95% O$_2$/5% CO$_2$. Coronal sections (250 µm) containing the PVN were obtained using a vibratome (Leica). Slices were allowed to recover for 15 min in 30 °C N-methyl-D-glucamine (NMDG)-recovery solution containing (in mM) 2.5 KCl, 25 NaHCO$_3$, 0.5 CaCl$_2$, 10 MgCl$_2$, 1.2 NaH$_2$PO$_4$, 25 glucose, 110 NMDG and 110 HCl, saturated with 95% O$_2$/5% CO$_2$. Following 1 h recovery in 30 °C artificial cerebrospinal fluid (aCSF) with NMDG, slices were incubated for 1 h in 30 °C aCSF containing (in mM) 126 NaCl, 2.5 KCl, 26 NaHCO$_3$, 2.5 CaCl$_2$, 1.5 MgCl$_2$, 1.25 NaH$_2$PO$_4$ and 10 glucose, saturated with 95% O$_2$/5% CO$_2$.

Electrophysiology. Data for experiments were acquired by multiple individuals. Only one individual was aware of the treatment of the animal during the experiment, while the others were blinded to the conditions. All recordings were obtained in aCSF containing picrotoxin (100 µM) at 30–32 °C, perfused at a rate of 1 ml min^{-1}. Neurons were visualized using an upright microscope fitted with differential interference contrast and epifluorescence optics and a camera. Borosilicate pipettes (2.5–4.5 mΩ) were filled with internal solution containing (in mM) 108 K-gluconate, 2 MgCl$_2$, 8 sodium-gluconate, 8 KCl, 1 K-EGTA, 4 K-ATP, 0.3 Na-GTP and 10 HEPES buffer. For current-clamp recordings, the initial membrane potential was −70 mV. To assess synaptic currents, cells were voltage-clamped at −70 mV. A monopolar aCSF-filled electrode placed in the vicinity of the cell (~20 µM) was used to evoke excitatory postsynaptic currents (EPSCs) 50 ms apart at 0.2 Hz intervals. The high-frequency stimulation consisted of four 100-Hz stimulations for 1 s every 10 s. Access resistance (<20 MΩ) was assessed every 3 min, and recordings were accepted for analysis if changes were <15%.

Viruses. A Cre-dependent adeno-associated virus (AAV) construct containing GCaMP6s (AAV9-CAG.Flex.GCaMP6s; Penn Vector Core) was injected into the PVN of Crh-IRES-Cre; Ai14 transgenic mice for the fiber photometry experiments. A recombinant AAV carrying Arch3.0-eYFP (rAAV2-EF1a-double floxed-Arch3.0-eYFP; 5×10^{11} genomic copies per ml; UNC Vector Core) or eYFP (Addgene plasmid 20296, pAAV-EF1a-double floxed-eYFP-WPRE-HGHpA; 5×10^{11} genomic copies per ml; Penn Vector Core) was used for optogenetic manipulations.

Stereotaxic surgery and optical fiber implantation. Mice were maintained under isoflurane anesthesia in the stereotaxic apparatus. A glass capillary containing viral vector was lowered into the brain (anterior–posterior (AP): −0.7 mm; lateral (L): −0.3 mm from the bregma; dorsal–ventral (DV): −4.5 mm from the dura). The virus was pressure injected with a Nanoject II apparatus (Drummond Scientific) in a total volume of 210 nl. For the single-fiber photometry experiments, 2 weeks were allowed for recovery; subsequently, a 400-µm diameter mono fiber optic cannula (Doric Lenses, MFC_400/430/0.48_5mm_MF2.5_FLT) was implanted dorsal to the PVN. The implant targeting was assisted by continuous monitoring of the fluorescence signal during the lowering of the optical fiber. For optogenetic experiments, mono fiber optic cannulas (Doric Lenses MFC_200/240-0.22_5mm_SMR_FLT) were stereotactically implanted. Both implantations were targeted to a similar position (for Arch3.0: AP: −0.7 mm; L: 0.0 mm from the bregma; DV: −4.0 mm; for GCaMP6s: AP: −0.7 mm; L: −0.2 mm from the bregma; DV: −4.0 mm from the dura) and were affixed to the skull with Metabond and dental cement. Mice were given 2 weeks to recover before the start of the experiment.

Fiber photometry recording. Fiber photometry was used to record calcium transients from CRH^{PVN} neurons in freely moving mice. After the recovery period, animals were handled for 5 min a day for three successive days and then habituated to the optic fiber in their homecage (15 min a day) for three additional days. We recorded 10 min of CRH^{PVN} neuron activity in the homecage immediately before and after each test. For fiber photometry data, mice were excluded if no pick-up-related calcium signal was observed in CRH^{PVN} neurons.

Two different fiber photometry systems were used. A fiber photometry system similar to that described in an earlier study[41] was used for all the looming-shadow tests and controllability experiments. Briefly, two excitation light-emitting diodes (LEDs; 470 nm M470F3 and 405 nm M405F1 from Thorlabs) were controlled by a RZ5P (Tucker-Davis Technology) processor running Synapse software (Tucker-Davis Technology). The LEDs were modulated at 211 Hz (470 nm) and 531 Hz

(405 nm) to avoid contamination from room lighting. Both LEDs were connected to a Doric Mini Cube filter set (FMC4_AE(405)_E(460–490)_F(500–550)_S) and the excitation light was directed to the animal via a mono fiber optic patchcord (Doric MFP_400/460/900-0.48_2m_FC/MF2.5). The power of the LEDs was adjusted to provide 30 µW at the end of the patch cord. The resulting signal was detected by a photoreceiver (NewPort model 2151) and demodulated by a RZ5P processor. For the tail-suspension experiments, a Doric fiber photometry system was used, which consisted of two excitation LEDs (465 nm and 405 nm from Doric) controlled by a LED driver and console running Doric Studio software (Doric Lenses). The LEDs were modulated and the resulting signal demodulated using lock-in amplification. Both LEDs were connected to a Doric Mini Cube filter set (FMC4_AE(405)_E(460-490)_F(500-550)_S) and the excitation light was directed to the animal via a mono fiber optical patchcord (Doric MFP_400/460/900-0.48_2m_FC/MF2.5). The power of the LEDs was adjusted to provide 30 µW at the end of the patch cord. The resulting signal was detected by a photoreceiver (NewPort model 2151).

Fiber photometry data analysis. Fluorescent signal data were processed in real time and acquired at a sampling rate of 1 kHz. Data were then exported to Matlab (MathWorks) for offline analysis using custom-written scripts. Briefly, the 470-nm and 405-nm data were first individually fit with a second-order polynomial curve, which was then subtracted to remove any artifacts due to bleaching. Next a least-squares linear fit was applied to the 405-nm data to align it with the 470-nm channel and then the change in fluorescence (ΔF) was calculated by subtracting the 405-nm Ca^{2+}-independent baseline signal from the 470-nm Ca^{2+}-dependant signal at each time point. Time-locked video of animal behavior was obtained during the photometry recordings. Within animal and group analyses were performed on the resulting z-score calculation using the following equation $z = (F - F_0)/\sigma F$, where F is the test signal, F_0 and σF are the mean and standard deviation of the basal signal, respectively[42]. For the peak detection analysis, a low-pass filter (5 Hz) was applied, and high-amplitude events were filtered and the median of the resultant trace was calculated. The peak detection threshold was set at two times the MAD. Scripts used to analyze fiber photometry and detect miniscope events are deposited at https://github.com/leomol/FPA and https://github.com/leomol/MSA.

Accelerometer recording and analysis. An analog accelerometer chip made by Analog Devices (ADXL335) was used to detect movement in the tail-suspension procedure. We purchased the breakout board, and directly provided one of the axes (x) as an analog input directly into the Doric system. Axial acceleration in the range of ±3 g is reported by the sensor as an analog voltage value. The Doric system then synchronously sampled from the photometer, the camera and the accelerometer data streams at the same rate. The accelerometer signal was validated using both ImageJ image subtraction analysis and compared to a manual annotation of struggling behavior. Struggle was assessed in two parts. First, a visual identification of a struggle bout, defined as a vigorous movement involving both hind and forelimbs usually accompanied by attempts to reach the tail by bending the body or crawling up toward its tail. Once a struggle bout was manually detected, the specific onset time of the movement was extracted from the accelerometer measurement to obtain a more precise time of onset of the behavior. The analyzed bouts were selected by a minimum time criteria of 2 s between bouts to allow for a stable calcium signal baseline between movement onsets. Immobility was defined as a lack of attempt to right itself.

Looming-shadow analysis. The onset of the escape was measured using two complementary methods. First, escape response onset was assessed by visual frame-by-frame analysis. The onset of the escape response was determined by noting the time of the exact video frame in which the animal initiated a movement toward the shelter within the 8-s interval that the looming stimulus was presented. Second, to automatically detect escape onset, the behavioral data were assessed using an image subtraction procedure from ImageJ and then analyzed using Matlab. The measure obtained as indicative of movement detection (in this case, looming-shadow-evoked escape) was the difference in pixels between the current and the previous sample detected. By measuring the median standard deviation from the baseline movement in every mouse, we determined that four times the MAD from the baseline was a reliable indicator of an escape movement. Again, we used an 8-s time limit for the automated escape behavior analysis.

Optogenetics. Following the recovery period, mice were handled on three consecutive days (5 min a day). Then, they were habituated for three additional days (15 min a day) to the fiber optic cable (200 µm core diameter, Doric Lenses) attached to the mono fiber optic cannula (no light). For experiments, the light source (for Arch3.0: 532 nm, LRS-0532-100-OP, Laserglow Technologies) was connected to the implanted ferrule with a fiber optic cable (200 µm core diameter, Doric Lenses). The lasers were controlled using a manually programmable Master 8 unit (A.M.P.I.). For Arch3.0, yellow light (15 mW laser intensity) was used continuously for the total time of the looming-shadow test duration (average 15 min).

Behavioral tests. Following fiber implantation, mice were individually housed for at least 2 weeks before behavioral testing. Before any behavioral manipulation,

mice were handled for 5 min each day for three successive days and habituated to the experimental room 1 h before testing. The apparatus was cleaned with a 70% ethanol solution to eliminate odor from other mice. All behaviors were recorded and scored offline by an experimenter blinded to the treatment conditions.

Looming-shadow test. Mice were placed in a 41 cm × 19 cm × 20.5 cm plastic arena with a 21-inch LCD monitor positioned above the arena facing downward to display a visual stimulus. At one end of the arena, a rudimentary shelter was provided (13 cm × 12 cm × 10 cm) under which the mice could hide. A lateral-top camera was placed to record the behavioral responses. Mice were habituated to the test arena for 3 days before the test (20 min a day). On the test day, following 3 min of habituation to the arena, five overhead looming visual stimuli were presented with a 1 min inter-trial interval. The looming stimulus was a 2-cm black disk that expanded to 20 cm in three distinct phases (Fig. 1b,c). The disk was present for 3 s, expanded to full size in 2 s and then was stable for 3 additional seconds. The following criteria were used to discriminate the different behaviors: (1) A flight response during the 8-s visual stimulus that resulted in the subject reaching the shelter, was classified as an escape or active behavior; (2) a response identified as absence of any movement except that related to breathing was classified as a passive or freezing behavior; (3) if the subject did not freeze, showed no change in ongoing behavior or made an escape attempt but did not reach the shelter during the 8-s stimulus presentation, it was classified as a non-responder.

FS stress. The FS protocol consisted of a 0.5-mA, 2-s FS delivered every 30 s for a period of 5 min in a FS chamber. Movement score during the FS was analyzed using ANY-maze software.

Tail suspension. Mice were suspended by the tail from a horizontal metal rod using regular laboratory tape. The procedure lasted for 10 min.

For the fiber photometry experiment in the looming-shadow test and the tail-suspension test, after the handling procedure and before the test habituation, all mice were also habituated for three additional days (15 min a day) to the fiber optic cable (Doric MFP_400/460/900-0.48_2m_FC/MF2.5) attached to the mono fiber optic cannula (no light).

Stress controllability. We used a custom-made shuttle box for the controllability training. For the behavioral experiments, a 42 cm × 21.5 cm × 20 cm cage was used. The apparatus was divided in two different compartments connected by a door (3.5 cm × 4 cm). For the fiber photometry experiments, a 22.5 cm × 23 cm × 40 cm cage was used. That apparatus was divided into two compartments (11 cm × 23 cm × 40 cm) that were connected by a 4.5-cm opening in the center wall. During the 3 days of training, mice were allowed to explore the shuttle box for 3 min. On each training day, they received 20 presentations of the training paradigm, which consisted of a 5-s tone (2-kHz tone delivered using custom-made software) followed by 3 s of a 0.3-mA FS (constant current). In the controllable group, if mice crossed over to the opposite side of the shuttle box anytime during the tone presentation (avoid) or FS administration (escape), the shock was terminated. If they remained in the same compartment during the trial, they received 3 s of FS. We recorded the time, number and order of the shock received for the controllable mice group and applied the same protocol to the uncontrollable pair. We assessed freezing behavior in the training context. Freezing behavior was analyzed using a stopwatch and was designated by the absence of any movement except respiratory movements. In the stress controllability experiments, mice that did not show a decrease in the number of shocks received at day 3 were excluded as a sign of not learning the task. For the fiber photometry experiment in the stress controllability experiments, after the handling procedure and before the training, all mice were also habituated to for three additional days (15 min a day) to the fiber optic cable (DORIC MFP_400/460/900-0.48_2m_FC/MF2.5) attached to the mono fiber optic cannula (no light) in the homecage.

For the controllability stress group, mice were tested in the looming-shadow test between 14 and 20 days after the last day of training and followed the same habituation protocol and test procedure as naive mice.

Conditioned tone exposure. Forty-eight hours after the last day of training, both controllable and uncontrollable mice were exposed to a novel environment. The novel environment consisted of an open arena (41 cm × 19 cm × 20.5 cm), and after 3 min of habituation, 5 conditioned tones, 8 s in duration, were presented with an interval of 52 s. Immobility behavior in this test was measured using ANY-maze v.6.18 software.

Decoder implementation. To classify the stress-training condition based on CRH[PVN] neuron activity, we used a Matlab-based massive feature extraction framework to automatically extract quantitative metrics from Ca^{2+} traces and subsequently trained a SVM–RBF kernel in Matlab using fivefold cross-validation[21,43]. Briefly, we grouped time traces by training day (day 1, day 2 and day 3) and created a labeled raw data matrix with class labels representing the stress-training condition (controllable versus uncontrollable). From that data matrix, we extracted 7,500+ features from each time trace using the HCSTA framework and used the *t*-distributed stochastic neighbor embedding algorithm to visualize nonlinear clustering in a lower-dimensional space. Next, we utilized the Classification Learner app in Matlab[43] to train a medium Gaussian SVM model (box constraint level = 1; Kernel

scale mode = Manual; Manual kernel scale = 87; Multiclass method: One-vs-One; Standardize data = 'Yes'; PCA: Disabled) with fivefold cross-validation for each case and evaluated the quality of the models using standard metrics (confusion matrix, area under the receiver operating characteristic curve).

Corticosterone immunoassay. Immediately after the last day of stress exposure in the controllability training session, blood from a 2-mm incision at the end of the tail vein was collected into ice-cold EDTA capillary tubes (Stardest) and centrifuged (8,000 r.p.m., 4 °C, 20 min). Aliquots of plasma were stored at −20 °C until assayed using a DetectX Corticosterone Immunoassay kit (Arbor Assay). Plasma samples were run in triplicate on the same day, and an average value per animal obtained per day. Different aliquots of plasma from the same animal were run on different days. Values were averaged across days per animal.

Statistics. GraphPad Prism 8.0 software was used for the statistical analyses. One-sample parametric *t*-test (two-tailed) or nonparametric Wilcoxon signed-rank test were used when comparing to the baseline period. When comparing means from two dependent groups or different time points, paired *t*-tests (two-tailed) were used. When comparing the means of two independent groups, parametric unpaired *t*-tests (two-tailed) or nonparametric Mann–Whitney *U*-tests (two-tailed) were used. When comparing the means of multiple groups, parametric repeated-measures, one-way or two-way analysis of variance (ANOVA) were used followed by Bonferroni corrections for multiple comparisons or nonparametric Kruskal–Wallis.

Reporting Summary. Further information on research design is available in the Nature Research Reporting Summary linked to this article.

Data availability
All relevant data and analysis tools are available upon reasonable request from the authors.

Code availability
Scripts used to analyze fiber photometry and detect miniscope events are deposited at https://github.com/leomol/FPA and https://github.com/leomol/MSA.

References
40. Cusulin, J. I. W., Füzesi, T., Watts, A. G. & Bains, J. S. Characterization of corticotropin-releasing hormone neurons in the paraventricular nucleus of the hypothalamus of Crh-IRES-cre mutant mice. *PLoS ONE* **8**, e64943 (2013).
41. Lerner, T. N. et al. Intact-brain analyses reveal distinct information carried by SNc dopamine subcircuits. *Cell* **162**, 635–647 (2015).
42. Guo, Q. et al. Multi-channel fiber photometry for population neuronal activity recording. *Biomed. Opt. Express* **6**, 3919–3931 (2015).
43. MATLAB and Classification Learner App v.R2018b (The MathWorks Inc., 2018).

Author contributions
N.D. designed and conducted experiments, analyzed data, prepared figures and wrote the manuscript. T.F. designed and conducted behavioral experiments, analyzed data and prepared figures. D.G.R. developed video and photometry analysis tools, analyzed behavioral data and reviewed the manuscript. N.P.R. and T.-L.S. conducted slice electrophysiology experiments and analyzed data. G.P. developed the accelerometer software and analysis, the artificial decoder and software for automating escape analysis. J.S.B. developed and supervised the project, analyzed data, constructed figures and wrote the manuscript.

Competing interests
The authors declare no competing interests.

Additional information
Extended data is available for this paper at https://doi.org/10.1038/s41593-020-0591-0.

Supplementary information is available for this paper at https://doi.org/10.1038/s41593-020-0591-0.

Correspondence and requests for materials should be addressed to J.S.B.

Peer review information *Nature Neuroscience* thanks Lieselot Carrette, Olivier George, and the other, anonymous, reviewer(s) for their contribution to the peer review of this work.

**Reprints and permissions information** is available at www.nature.com/reprints.
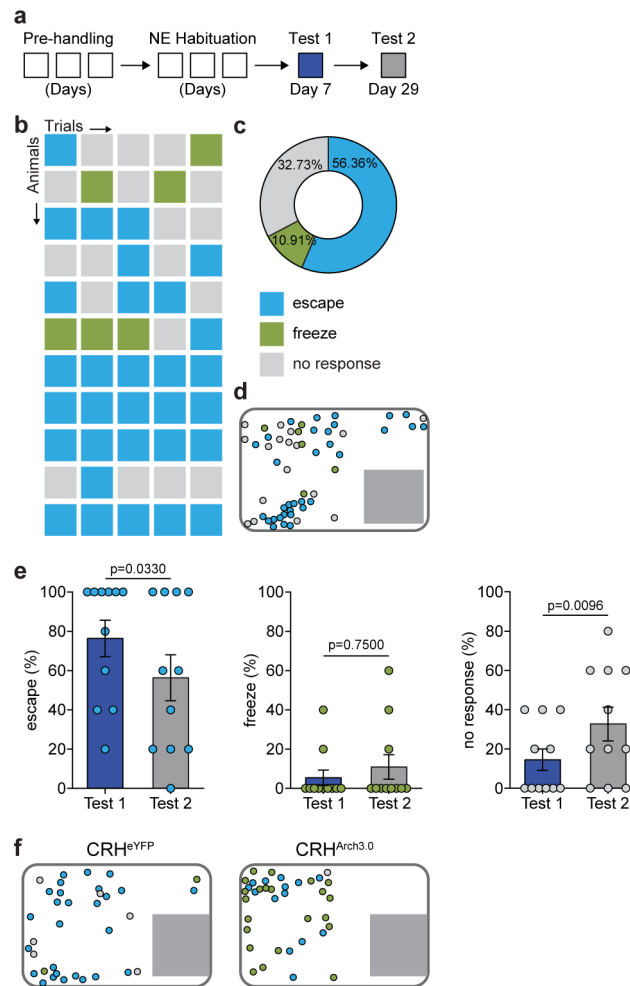
Extended Data Fig. 1 | Prior experience changes defensive strategy. a, Protocol for the second exposure to looming-shadow test. **b**, Behavioral analysis showing individual trials (trials/mice, n = 55, N = 11) and **c**, summary of all trials for the 3 behavioral outputs analyzed. **d**, Representation of the starting point of subject in each trial for the second exposure to the looming-shadow test. **e**, Data compiled and presented as fraction of trials showing a given behavior in a mouse. Escape (N = 11, Paired t-test, two tailed t(10) = 2.472, p = 0.0330, 95% CI: 1.973 to 38.03), freeze (Wilcox test, two-tailed, w = −3.000, p = 0.750), and no response (Paired t-test, two-tailed, t(10) = 3.194, p = 0.0096, 95% CI: −30.86 to −5.50). **f**, Representation of the starting point of subject in each trial for the photoinhibition experiment (left CRH^{eYFP}, right CRH$^{Arch3.0}$). Data shown are means ± s.e.m.
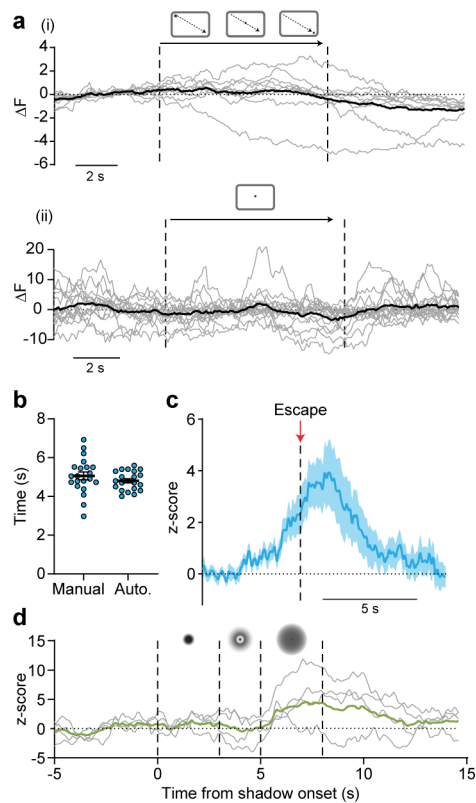
Extended Data Fig. 2 | Relationship between GCaMP signal and visual stimulus assessed using different parameters. a, (i) Individual traces (gray) and mean (overlaid black) of CRH[PVN] activity in response to an object that tracks in a horizontal plane across the sky but does not advance (trials/mice, n=9, N=3). The length of the stimulus was 8 s and it was moving at a constant speed of 6 cm/s. (ii) Individual traces (gray) and mean (overlaid black) of CRH[PVN] activity in response to an object that remains static in a horizontal plane across the sky for the duration of the experiment (trials/mice, n=15, N=3) **b**, Individual traces (gray) and mean (overlaid green) of CRH[PVN] activity in response to shadow presentation corresponding to trials resulting in a freezing behavior for Naïve mice (trials/mice, n=4, N=3). **c**, Comparison between manual vs automated assessment of escape onset in the looming-shadow test (Paired t-test, two tailed, t(20)=1.027, p=0.3169, 95% CI −0.7580 to 0.2580). **d**, Average z-score of CRH[PVN] calcium response with individual trials time-locked to the onset of the escape when assessed manually using a frame by frame approach. Escape response indicated by dashed line and red arrow (trials/mice n=21, N=5). Solid lines represent average, and the shaded areas indicate SEM. Data shown are means ± s.e.m.
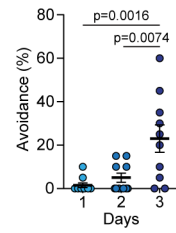
Extended Data Fig. 3 | Avoidance behavior during controllable stress training. Avoidance behavior in controllable group (N = 10, day 1 to day 3, repeated measure ANOVA, $F_{(2,18)}$ = 10.17, p = 0.0011, Bonferroni's multiple comparisons test, Day1 vs day 2 p > 0.999, 95% CI −17.00 to 10.00. Day 2 vs day 3 p = 0.0074, 95% CI −35.00 to −8.00. Day 3 vs day 1 p = 0.0016, 95% CI −31.50 to −4.50). Data shown are means ± s.e.m.
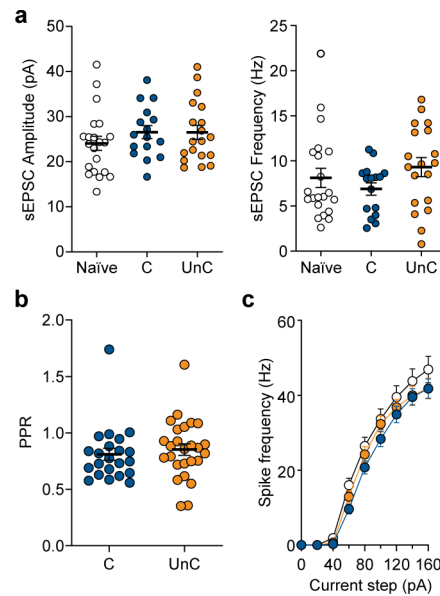
Extended Data Fig. 4 | Effects of controllability training on basal glutamate transmission and intrinsic excitability of CRH^{PVN} neurons. a, sEPSC amplitude and frequency for naïve, controllable and uncontrollable stress 24 h after the last training session (cells/mice, Naive = 21/4, Controllable = 16/5, Uncontrollable = 19/5; amplitude, one-way ANOVA, f(2,53) = 0.8868, p = 0.4180, Bonferroni's multiple comparison, Naïve vs controllable p = 0.7944, 95% CI −2.966 to 7.935. Naïve vs Uncontrollable p = 0.7743, 95% CI −2.796 to 7.936. Controllable vs Uncontrollable p > 0.999, 95% CI −5.497 to 5.654; frequency, one-way ANOVA, F(2,53) = 1.405, p = 0.2544, Bonferroni's multiple comparison, Naïve vs controllable p = 0.6639, 95% CI −4.640 to 2.188. Naïve vs Uncontrollable p = 0.6509, 95% CI −2.059 to 4.456. Controllable vs Uncontrollable p = 0.2244, 95% CI −5.915 to 1.067). **b**, Bar graph showing no significant changes in baseline PPR between groups (cells/mice, Controllable = 21/9, Uncontrollable = 25/10, Unpaired t-test, two-tailed, t(44) = 1.037, p = 0.3053, 95% CI −0.05364 to 0.1674). **c**, F-I plot shows spike frequency for each depolarizing current step (cells/mice, Naive = 18/4, Controllable = 30/5, Uncontrollable = 27/5 -2way ANOVA current step x group F(18,648) = 0.8444, p = 0.6476). Data shown are means ± s.e.m.
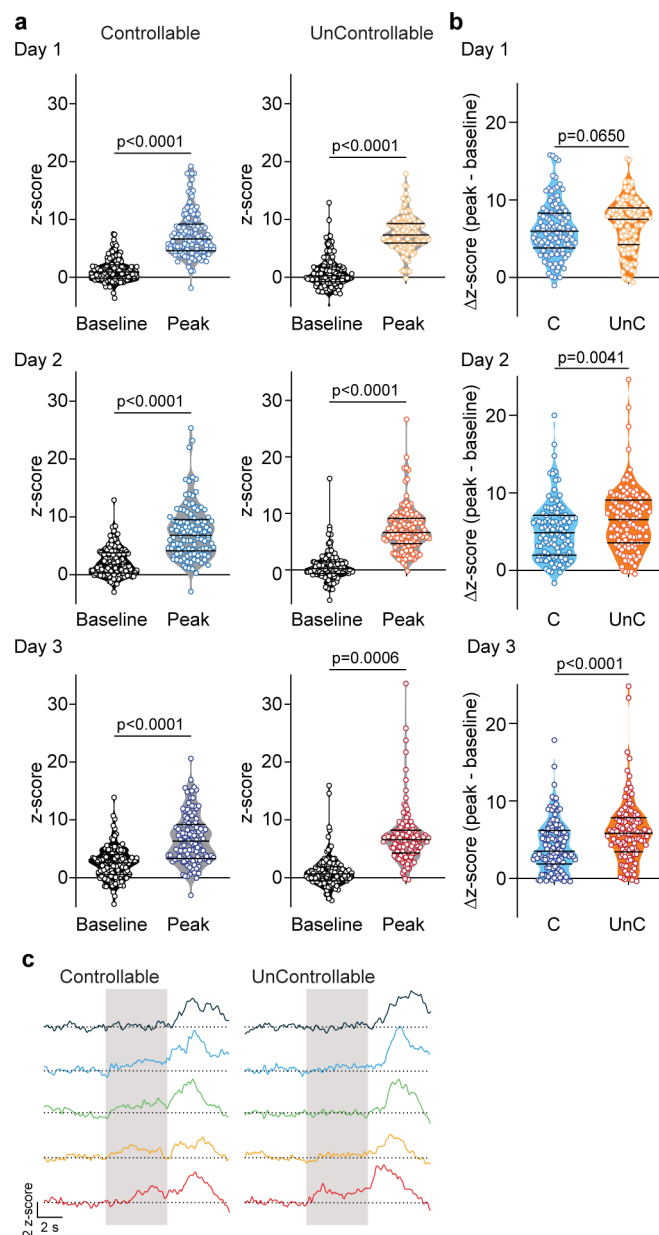
Extended Data Fig. 5 | Peak GCaMP responses to footshock following controllable and uncontrollable stress. a, Individual z-scores of baseline (shock onset) and footshock peak values for controllable (right, blue circles, Day 1 trials/mice = 120/6; Baseline min = −3.369, 25% = −0.1015, med = 1.118, 75% = 2.118, max = 7.730. FS peak min = −1.849, 25% = 4.602, med = 6.639, 75% = 9.195, max = 19.19; Wilcoxon signed rank test, two-tailed, W = 7248, p < 0.0001. Day 2 trials/mice = 114/6; Baseline min = −2.906, 25% = 0.4915, med = 1.593, 75% = 3.993, max = 13.14. FS peak min = −2.906, 25% = 4.155, med = 6.818, 75% = 9.533, max = 25.36; Wilcoxon signed rank test, two-tailed, W = 5430, p < 0.0001. Day 3 trials/mice = 119/6; Baseline min = −4.187, 25% = 0.5293, med = 2.544, 75% = 3.808, max = 14.82. FS peak min = −3.033, 25% = 3.302, med = 6.333, 75% = 9.212, max = 20.61; Wilcoxon signed rank test, W = 6399, p < 0.0001) and uncontrollable (orange circles, Day 1 trials/mice = 120/6; Baseline min = −5.375, 25% = −0.6542, med = 0.4421, 75% = 1.974, max = 12.61. FS peak min = −2.018, 25% = 5.927, med = 7.320, 75% = 9.287, max = 17.91; Wilcoxon signed rank test, two-tailed, W = 7230, p < 0.0001. Day 2 trials/mice = 119/6; Baseline min = −5.068, 25% = 0.6244, med = 0.3252, 75% = 1.568, max = 17.68. FS peak min = −0.218, 25% = 4.628, med = 6.598, 75% = 9.112, max = 26.66; Wilcoxon signed rank test, two-tailed, W = 7009, p < 0.0001. Day 3 trials/mice = 120/6; Baseline min = −3.594, 25% = −0.5115, med = 0.6376, 75% = 2.253, max = 16.58. FS peak min = −0.3636, 25% = 4.288, med = 6.584, 75% = 8.212, max = 33.54; Wilcoxon signed rank test, two-tailed, W = 5430, p = 0.0006) group. **b**, Individual delta z-scores (footshock - baseline) on day 1 (Controllable trials/mice = 120/6; min = -1.061, 25% = 3.809, med = 5.967, 75% = 8.262, max = 15.79. Uncontrollable trials/mice 120/6. min = -0.667, 25% = 4.222, med = 7.493, 75% = 8.956, max = 15.31; Mann-Whitney test, two tailed, U = 62.7, p = 0.0650), day 2 (Controllable trials/mice = 114/6; min = -1.667, 25% = 1.948, med = 4.855, 75% = 7.101, max = 19.22. Uncontrollable trials/mice = 119/6; min = -0.4561, 25% = 3.558, med = 6.533, 75% = 9.064, max = 24.63; Mann-Whitney test, two tailed, U = 5307, p = 0.0041) and day 3 (Controllable trials/mice = 120/6; min = -0.4106, 25% = 1.844, med = 3.499, 75% = 6.173, max = 17.86. Uncontrollable trials/mice = 120/6; min = -0.3787, 25% = 3.421, med = 5.809, 75% = 7.824, max = 24.80; Mann-Whitney test, two tailed, U = 5014, p < 0.0001). **c**, Average CRH^{PVN} activity on day 1 for both controllable and uncontrollable groups on trial 3, 5, 15, 18 and 20 (n = 6). Data shown in the violin plots are median, 25% and 75% percentile (black bars).
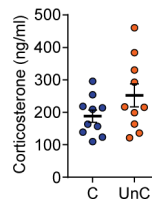
Extended Data Fig. 6 | Circulating corticosterone levels after controllability training. Corticosterone levels after the last day of training of controllable (N = 10) and uncontrollable (N = 10) stress protocol (Unpaired t-test, two-tailed, t(19) = 1.586, p = 0.1301, 95% CI: -147.9 to 20.65). Data shown are means ± s.e.m.
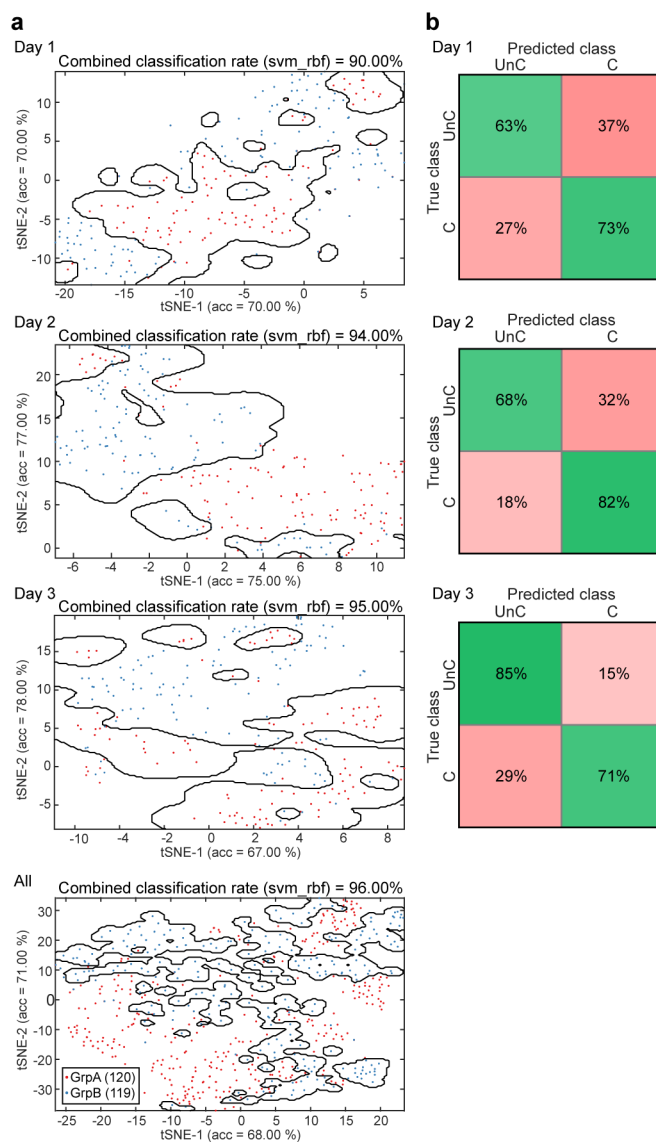
Extended Data Fig. 7 | Non-linear clustering visualization in lower dimensional space. a, Visualization of the data matrix using non-linear clustering in a lower-dimensional space based on the 2 main features extracted from the calcium traces. From top to bottom: day 1 alone, day 2 alone, day 3 alone, all training days combined. **b**, Confusion matrices showing the classification accuracy (ratio of correct predictions to total predictions made) of the trained decoder from (top to bottom) day 1 to day 3.
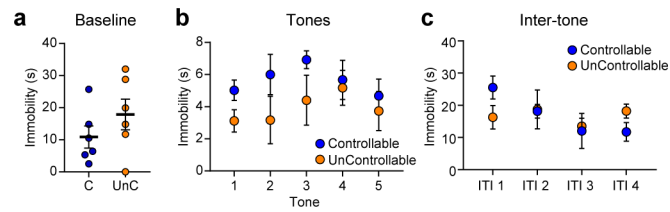
Extended Data Fig. 8 | Immobility in response to controllability training. Immobility during: (**a**) baseline period (5 min before the tone presentation, unpaired t-test, two-tailed, t(10) = 1.185, p = 0.2636, 95% CI -6.161 to 20.16), (**b**) during tone presentation, 8 s stimulus presentation (two-way ANOVA, tone x group interaction f(4,40) = 0.5399, p = 0.7073) and (**c**) between tones (two-way ANOVA, tone x group interaction f(3,30) = 1.823, p = 0.1642). Inter-tone-interval (ITI) = 52 s, (N = 6 each group). Data shown are means ± s.e.m.
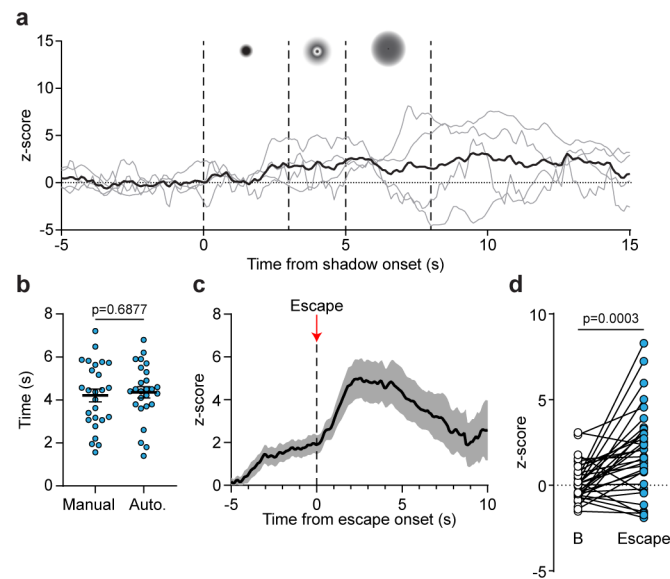
Extended Data Fig. 9 | Additional photometry data analysis for looming shadow tests following controllability training. a, Non-responders in uncontrollable group showing individual traces (gray) and average z-score (black) of CRH[PVN] calcium response during visual stimulus presentation (trials/mice = 4/3). **b**, Comparison between manual (frame by frame), and automated analysis of the escape reaction time (n = 26, ERT, Paired t-test, two-tailed, t(25) = 0.4067, p = 0.6877, 95% CI -0.5929 to 0.8847). **c**, Average z-score of CRH[PVN] calcium response with individual trials time-locked to the onset of the escape. Escape response indicated by dashed line and red arrow (trials/mice n = 33, N = 9). **d**, Individual z-score values at the baseline (white circles) and at flight response initiation (blue circles, trials/mice n = 33, N = 9; two-tailed paired t-test, t(32) = 4.025, p = 0.0003, 95% CI 0.8558 to 2.610). Solid lines represent average, and the shaded areas indicate s.e.m. Data shown are means ± s.e.m.
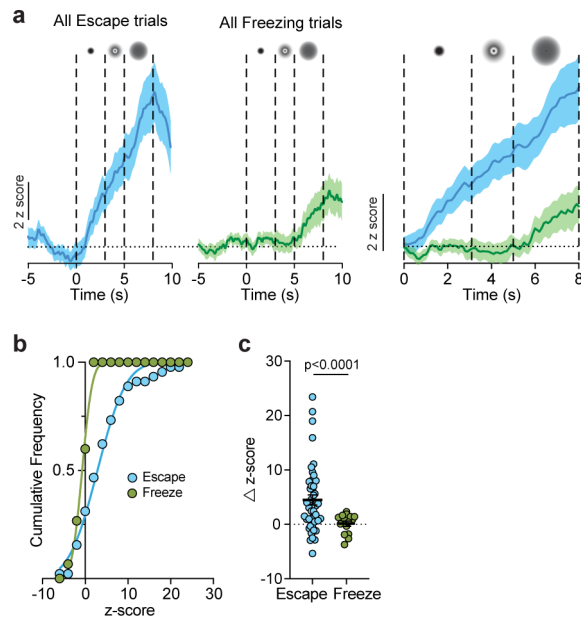
Extended Data Fig. 10 | Compiled GCaMP data across experiments from all escape trials and all freeze trials. a, Average z-score of CRH[PVN] calcium response with all individual trials time-locked to the onset of stimulus. Left panel shows all trials (naïve, controllable and uncontrollable stress; n = 55 trials) that showed an escape response; middle panel shows all trials that showed a freezing response; n = 16 trials). Right panel shows the overlaid responses from escapers and freezers during the shadow presentation. **b**, Cumulative distributions of z-scores at the end of shadow expansion (5 s from stimulus onset). **c**, z scores from escape (n = 55) and freeze (n = 16) trails at the 5 s mark of shadow presentation (two-tailed unpaired t-test, Welch's correction; t(57.55) = 4.184, p < 0.0001, 95% CI 2.266 to 6.426). Data shown are means ± s.e.m.

natureresearch

Corresponding author(s):   Jaideep S. Bains

Last updated by author(s):   2019/12/31

Reporting Summary

Nature Research wishes to improve the reproducibility of the work that we publish. This form provides structure for consistency and transparency in reporting. For further information on Nature Research policies, see Authors & Referees and the Editorial Policy Checklist.

Statistics

For all statistical analyses, confirm that the following items are present in the figure legend, table legend, main text, or Methods section.

n/a	Confirmed	
☐	☒	The exact sample size (n) for each experimental group/condition, given as a discrete number and unit of measurement
☐	☒	A statement on whether measurements were taken from distinct samples or whether the same sample was measured repeatedly
☐	☒	The statistical test(s) used AND whether they are one- or two-sided *Only common tests should be described solely by name; describe more complex techniques in the Methods section.*
☒	☐	A description of all covariates tested
☐	☒	A description of any assumptions or corrections, such as tests of normality and adjustment for multiple comparisons
☐	☒	A full description of the statistical parameters including central tendency (e.g. means) or other basic estimates (e.g. regression coefficient) AND variation (e.g. standard deviation) or associated estimates of uncertainty (e.g. confidence intervals)
☐	☒	For null hypothesis testing, the test statistic (e.g. F, t, r) with confidence intervals, effect sizes, degrees of freedom and P value noted *Give P values as exact values whenever suitable.*
☒	☐	For Bayesian analysis, information on the choice of priors and Markov chain Monte Carlo settings
☒	☐	For hierarchical and complex designs, identification of the appropriate level for tests and full reporting of outcomes
☒	☐	Estimates of effect sizes (e.g. Cohen's d, Pearson's r), indicating how they were calculated

Our web collection on statistics for biologists contains articles on many of the points above.

Software and code

Policy information about availability of computer code

Data collection	TDT Synapse (version 84-34769P, Tucker-Davis Technology) and Doric Studio (version V5.3.3.6, DORIC) software was used for the fiber photometry data collection. For the electrophysiological data, signals were amplified using Multiclamp 700B amplifier (Molecular Devices), low-pass filtered at 1 kHz and digitized at 10 kHz using Digidata 1440 (Molecular Devices). Data was recorded (pClamp 10.2, Molecular Devices) for offline analysis. For the accelerometer data, an analog accelerometer chip made by Analog Devices (ADXL335) was used to detect movement in the tail suspension procedure. A breakout board (Arduino UNO) directly provided one of the axes (x) as an analog input directly into the Doric Studio system. For the automated behavioral data analysis we used ImageJ (version 1.52p).
Data analysis	MATLAB R2018a was used to analyze fiber photometry data, automated behavioral data and for the Classification Learner. Briefly for the photometry data analysis 470nm and 405nm data were first individually fit with a second order polynomial curve which was then subtracted to remove any artifacts due to bleaching. Next a least-squares linear fit was applied to the 405nm in order to align it with the 470nm channel and then the change in fluorescence (ΔF) was calculated by subtracting the 405nm Ca2+ independent baseline signal from the 470nm Ca2+ dependent signal at each time point. For the peak detection analysis a low pass filter (5Hz) was applied and high amplitude events were filtered and the median of the resultant trace was calculated. The peak detection threshold was set. Regarding the behavioral analysis of the looming shadow, the median standard deviation from the baseline movement in every mouse, was measured and then we determined a threshold from the baseline that was a reliable indicator of an escape movement. For the Classification learner, MATLAB-based massive feature extraction framework was used to automatically extract quantitative metrics from Ca2+ traces and subsequently trained a Support Vector Machine with a radial basis function kernel (SVM-RBF) in MATLAB using 5-fold cross-validation. Anymaze software was used to assess immobility behavior. Clampfit 10.7 was used to analyze the electrophysiological data. For the statistical analysis, GraphPad Prism 8 were used to analyze all the data.

For manuscripts utilizing custom algorithms or software that are central to the research but not yet described in published literature, software must be made available to editors/reviewers. We strongly encourage code deposition in a community repository (e.g. GitHub). See the Nature Research guidelines for submitting code & software for further information.

Data

All relevant data and analysis tools are available upon reasonable request from the authors.

Field-specific reporting

Please select the one below that is the best fit for your research. If you are not sure, read the appropriate sections before making your selection.

☒ Life sciences ☐ Behavioural & social sciences ☐ Ecological, evolutionary & environmental sciences

For a reference copy of the document with all sections, see nature.com/documents/nr-reporting-summary-flat.pdf

Life sciences study design

All studies must disclose on these points even when the disclosure is negative.

Sample size	Sample sizes were based on previous experiments conducted by us and other labs that used similar techniques.
Data exclusions	For fiber photometry data, mice were excluded if no pick-up related calcium signal was observed in PVN CRH neurons. In the stress controllability experiments, mice that did not show a decrease in shock received at day 3 were excluded as a sign of not learning in the task.
Replication	Our observations that PVN CRH neuron activity is linked to innate and escape behavior has been successfully reproduced in multiples cohorts of mice. Also similar observations have been made by other lab members.
Randomization	Mice were randomly selected. If multiple mice were used from one litter the mice were spread across experimental groups to avoid a litter effect.
Blinding	Due to the nature of the experiments, one experimenter overseeing the experiment could not be blind to the experimental groups. But the operationalization of the behavioral variables minimize the interferences.

Reporting for specific materials, systems and methods

We require information from authors about some types of materials, experimental systems and methods used in many studies. Here, indicate whether each material, system or method listed is relevant to your study. If you are not sure if a list item applies to your research, read the appropriate section before selecting a response.

Materials & experimental systems

n/a	Involved in the study
☒	☐ Antibodies
☒	☐ Eukaryotic cell lines
☒	☐ Palaeontology
☐	☒ Animals and other organisms
☒	☐ Human research participants
☒	☐ Clinical data

Methods

n/a	Involved in the study
☒	☐ ChIP-seq
☒	☐ Flow cytometry
☒	☐ MRI-based neuroimaging

Animals and other organisms

Laboratory animals	Male and female CRH-IRES-Cre; Ai14 mice in which CRH neurons express td-Tomato fluorophore were used (CRH-IRES-Cre X td-Tomato). Mice were 6-8 weeks old at the time of the surgery. For naive experiment in looming-shadow test, test C57BL/6-Elite male mouse obtained from Charles River were used (6-8 weeks old).
Wild animals	The study did not involved wild animals
Field-collected samples	The study did not involved field-collected samples
Ethics oversight	University of Calgary Animal Care and Use Committee

Note that full information on the approval of the study protocol must also be provided in the manuscript.